



# Impact of Arctic sea ice on the boreal summer intraseasonal oscillation

Zihuang Xie<sup>1</sup> · Yao Ha<sup>1,2</sup> · Yimin Zhu<sup>1,2</sup> · Yijia Hu<sup>1</sup> · Zhong Zhong<sup>2,3</sup>

Received: 11 January 2024 / Accepted: 18 March 2024  
© The Author(s) 2024

## Abstract

This study investigates the relationship between sea ice concentration (SIC) in the Arctic Ocean and the Boreal Summer Intraseasonal Oscillation (BSISO) from 1991 to 2020 and its underlying mechanism. A significantly positive (negative) correlation was found between the frequency of phase 7 (3) of BSISO1 (30–60 d) and the preceding winter SIC, which is located the north of the East Siberian-Beaufort Sea (ESBS). Compared with low-SIC years, the conditions including north-easterly vertical wind shear, an enhanced ascending branch of the anomalous Walker circulation, an eastward water vapour transport channel, and an increased humidity gradient induce active convection over the Philippine Sea in high-SIC years, which benefits (hinders) to phase 7 (3) of BSISO1. The positive SIC anomaly during the transition from winter to spring influences local temperature and pressure through anomalous local sensible heat flux. This anomaly induces wave activity flux from the ESBS, which converges over the Bering Sea, enhancing the Aleutian Low (AL). Subsequently, the AL triggers an anomalous subtropical anticyclone through wave-mean flow interaction in the North Pacific. Due to southerly wind stress and increased sea surface heat flux, positive sea surface temperature anomalies near Japan persist in the summer, heating the lower troposphere and increasing baroclinicity. Significant positive geopotential heights and anticyclone anomalies occur over Japan, accompanied by a negative vorticity anomaly. The enhanced ascending motion over the Philippine Sea, facilitated by Ekman pumping, favours convection and influences the frequency of phases 7 and 3.

**Keywords** Arctic sea ice · Boreal summer intraseasonal oscillation · Aleutian low · SST warming near Japan

## 1 Introduction

The Arctic, located in a high-latitude cold region, is a major heat absorber for Earth. The Arctic cryosphere plays a crucial role in Earth's climate system, with high sensitivity and long-term impact. It has undergone experienced changes in recent decades (Cohen et al. 2014). Globally, surface temperatures have steadily increased over the past few decades.

From 2011 to 2020, the average global surface temperature was 1.09 °C higher than between 1850 and 1900. The temperature changes have led to unprecedented transformations in the Arctic, which has warmed more than twice as fast as the global average since the late twentieth century—a phenomenon known as Arctic amplification (Cohen et al. 2014, 2020; Coumou et al. 2018; Rantanen et al. 2022). The Arctic's rapid climate changes have far-reaching implications, affecting polar regions, weather, and climate patterns in mid-to-low-latitude regions (Screen and Simmonds 2013; Cohen et al. 2014, 2020; Vihma 2014).

Sea ice is crucial for the transfer of heat, momentum, water vapour and other substances between the atmosphere and oceans in the Arctic. Previous research links Arctic amplification to temperature feedback, sea ice albedo feedback and reduced sea ice leading to heat transfer from the ocean to the atmosphere (Holland and Bitz 2003; Bintanja and Van Der Linden 2013; Pithan and Mauritsen 2014; Vihma 2014; Boeke and Taylor 2018; Sang et al. 2022). Arctic sea ice is regarded as an indicator of climate change both in the Arctic and globally. It has drastically changed

---

✉ Yao Ha  
hayao1986@yeah.net

✉ Yimin Zhu  
zhuym@21cn.com

<sup>1</sup> College of Meteorology and Oceanography, National University of Defense Technology, Changsha 410073, China

<sup>2</sup> Jiangsu Collaborative Innovation Center for Climate Change, School of Atmospheric Sciences, Nanjing University, Nanjing 210023, China

<sup>3</sup> Key Laboratory for Virtual Geographic Environment, School of Geography Science, Nanjing Normal University, Nanjing 210023, China

in recent decades, frequently breaking historic lows and its cover range shrinking to 3.8% per decade (Comiso and Hall 2014). In 2007, the Arctic sea ice area reached a minimum of 4.13 million square meters (Perovich et al. 2008). In 2012, satellite observations recorded an unprecedented ice extent, merely half the average minimum cover area between 1979 and 2000 (Yuan et al. 2018). Subsequently, 2020 was the second smallest year for Arctic sea ice coverage (Wei et al. 2021). Numerical models project a future scenario of an ice-free Arctic Ocean during summer and autumn (Holland et al. 2006; Sigmond et al. 2018), although these models often underestimate the actual rate of sea ice melting (Stroeve et al. 2007; Rosenblum and Eisenman 2017).

Arctic sea ice significantly influences local and global climate through interactions with the atmosphere and oceans. Numerous studies have shown its impact on winter atmospheric circulation in mid- to high latitudes and the underlying physical processes (Honda et al. 2009; Liu et al. 2012; Yang et al. 2020; Li et al. 2021, 2023). Observational data and model simulations by Honda et al. (2009) showed that turbulent heat flux anomaly caused by autumn sea ice anomalies in the Barents-Kara Sea enhanced the Siberian High by triggering stationary Rossby waves, leading to colder temperatures in the Far East during winter. Liu et al. (2012) found that reduced Arctic sea ice results in an enhanced source of water vapour and a more meridional atmospheric circulation in the mid-latitudes, increasing blocking and cold wave events. Moreover, the relationship between Arctic sea ice and summer atmospheric circulation in the mid-to-high latitudes of the Eurasian continent has also been explored (Wu et al. 2009a, b, 2013; Li and Leung 2013; Cohen et al. 2014; Mori et al. 2014; Vihma 2014). Atmospheric circulation changes may further influence extreme weather events in mid-to-high latitudes (Francis and Vavrus 2012; Chripko et al. 2021; Yao et al. 2023). Studies have also shown that Arctic sea ice loss enhances warming in the eastern equatorial Pacific and intensifies the Intertropical Convergence Zone (England et al. 2020).

Additionally, Arctic sea ice concentration (SIC) anomalies may induce El Niño-like warming in the central tropical Pacific, potentially leading to more frequent strong El Niño events (Kim et al. 2020; Liu et al. 2022). Furthermore, the variations in Arctic sea ice have been linked to the frequency, genesis potential index, and accumulated energy of tropical cyclones in the western North Pacific (Ma et al. 2014; Fu et al. 2021; Chen et al. 2023a). However, some studies argued that there was no consensus on whether Arctic warming affects mid or low-latitudes (Screen et al. 2014; Barnes and Screen 2015).

Intraseasonal oscillation (ISO) is a periodic phenomenon lasting 10–90 days in the atmosphere. Although ISO has also been observed at mid-to-high latitudes, many studies have mainly focused on the tropics (Anderson and Rosen 1983;

Pancheva 2003; Huang et al. 2015; Yang and Li 2016; Wang et al. 2022). The tropical ISO, or the Madden-Julian Oscillation (MJO, 1971, 1972), is the strongest intraseasonal signal in the tropical atmosphere throughout the year, executing impact on various spatiotemporal scales (Zhang 2013; Serra et al. 2014). It involves coupling and eastward propagation between large-scale Kelvin-Rossby wave structures and convection throughout the year. However, due to the seasonal cycle in boundary conditions and associated circulations, such typical behavior is most pronounced during boreal winter and another mode emerges during boreal summer (Madden and Julian 1994; Zhang 2005; Kikuchi 2021). In summer, the main centres of convection variability associated with the tropical ISO shift northward from the equator to 10°–20°N, resulting in more complex propagation patterns (Lee et al. 2013; Chen and Wang 2021). In addition to MJO-like eastward propagation along the equator (Hu et al. 2023), the summer tropical ISO exhibits a northward/northeastward propagation component over the Indian summer monsoon region and the western North Pacific-East Asia region (Kemball-Cook and Wang 2001; Lawrence and Webster 2002; Annamalai and Sperber 2005; Chu et al. 2012; Li et al. 2023). This distinct mode, different from MJO, is known as the Boreal Summer Intraseasonal Oscillation (BSISO) (Wang et al. 2023).

For the ASM and the global monsoon, the BSISO is recognized as the primary source driving short-term climate variations at various spatiotemporal scales (Webster et al. 1998; Wang and Ding 2008; Kikuchi 2021). Previous studies have shown that the BSISO may impact the onset of the ASM, as well as the active-break cycles, seasonal mean, genesis, and track of typhoons (Kang et al. 1999; Krishnamurthy and Shukla 2008; Ding and Wang 2009; Nakano et al. 2021; Hu et al. 2022; Wei et al. 2022). Moreover, it can contribute to seasonal climate predictions related to precipitation and extratropical atmospheric circulation (Ding and Wang 2005; Wang et al. 2009, 2012; Lee et al. 2010).

Previous studies have shown that the BSISO consists of two components in frequency bands, corresponding to different atmospheric modes and propagation characteristics (Wang et al. 2005; Kikuchi and Wang 2010; Lee et al. 2013; Wu and Cao 2017). For example, the BSISO can be divided into BSISO1 and BSISO2 by performing multivariate empirical orthogonal function decomposition on daily data from May to October of outgoing long-wave radiation (OLR) and 850 hPa zonal wind on a particular area (40°–160°E, 10° S–40°N) (Lee et al. 2013). The BSISO1 is associated with northward-propagating variability that often coincides with the eastward movement of the MJO, having quasi-oscillating periods lasting 30–60 days. On the other hand, the BSISO2 mainly captures northward or northwestward-propagating variability with periods spanning from 10 to 30 days, particularly

during the pre-monsoon and monsoon-onset seasons. The unique climatology of the Asian Summer Monsoon (ASM) region significantly influences the evolution and propagation of the BSISO. The thermal conditions, including poleward surface temperature and humidity gradients, in the ASM region result in similar distributions of convective instability and moist static energy. These conditions create a favorable environment for the northward and eastward propagation of the BSISO (Ajayamohan and Goswami 2007; Jiang et al. 2004; Li et al. 2013; Hu et al. 2023). As for the dynamic factors, the significant easterly vertical wind shear in the ASM region is beneficial for the northward propagation of BSISO, and its mechanism has been systematically explained (Wang and Xie 1996; Xie and Wang 1996; Jiang et al. 2004; Wang et al. 2006). Some studies have discussed the effect of background northerly wind shear on the northward propagation, propagation speed, and stability of the BSISO (Bellon and Sobel 2008; Dixit and Srinivasan 2011). Moreover, the southwesterly monsoon in the ASM region can directly transport water vapour and induce northward convection (DeMott et al. 2013).

As previously mentioned, some studies have explored the impact of the Arctic on the tropics, and there are also some encouraging developments regarding the effect of the Arctic on MJO. Flatau and Kim (2013) showed that a persistent Arctic Oscillation anomaly appears to influence the convection in the tropical belt and impact the distribution of MJO-preferred phases by the sea surface temperature (SST) changes. The occurrences of MJO phases 6 and 7 have been proven to significantly increase during around 20 days after the onset of Northern Hemisphere (NH) stratospheric sudden warmings (Wang et al. 2020). The exact responses of tropical convection to NH extreme stratospheric polar vortex events have also been investigated (Wang et al. 2022). However, there is a research gap concerning the impact of the Arctic on BSISO, particularly Arctic sea ice. Given the significant role of the BSISO in weather and climate, this study aims to investigate the potential connection between Arctic SIC and the subsequent BSISO. Additionally, the study explores the underlying physical mechanisms through which Arctic SIC influences the BSISO in the ASM region.

The remainder of this paper is organized as follows: Section 2 introduces datasets, indices, and analytical methods. The statistical relationships between the Arctic SIC and BSISO phases are presented in Section 3. Section 4 explores the characteristics of the circulation and water vapour anomalies associated with Arctic SIC in the ASM region. Section 5 elaborates on the possible mechanisms by which winter Arctic SIC affects the BSISO. Finally, a summary and discussion are presented in Section 6.

## 2 Data and methods

The data utilized in this study include the following: 1) Daily and monthly ERA5 datasets from the European Centre for Medium-range Weather Forecasts (ECMWF). These datasets comprise air temperature, geopotential height, horizontal wind, specific humidity, etc. (Hersbach et al. 2020); 2) Monthly SST and SIC datasets from the Met Office Hadley Center, with a horizontal resolution of  $1.0^\circ \times 1.0^\circ$ . These datasets have been detrended to exclude the possible impact of global warming; 3) Daily and monthly OLR datasets from the National Oceanic and Atmospheric Administration (NOAA), with a horizontal resolution of  $2.5^\circ \times 2.5^\circ$ ; 4) monthly Niño3.4 index from NOAA; 5) Daily BSISO indices, including BSISO1 and BSISO2, were obtained from the Asia-Pacific Economic Cooperation Climate Center (APCC). Compared with the real-time multivariate MJO (RMM) index proposed by Wheeler and Hendon (2004), the BSISO1 and BSISO2 indices are capable of describing a large fraction of the total intraseasonal variability in the ASM region and better represent northward/northwestward propagation (Lee et al. 2013). The BSISO occurs from May to October and is mainly active from June to August (JJA). Moreover, there is a lag effect in sea ice changes, which is a slow process compared to the atmosphere. Some studies have proved that winter and spring Arctic sea ice could lead to climate changes in the following summer (Chen et al. 2023a; Wu et al. 2009a, b, 2013). Therefore, this study focused on the possible impact of the preceding winter and spring Arctic sea ice on the JJA BSISO. All cases were used in the study regardless of the amplitude of the BSISO indices. Considering the global interdecadal changes in the 1990s, the study period was selected as 1991 to 2020, which was also a basic climatology.

Wave activity flux (WAF) is commonly used in atmospheric dynamics to diagnose the propagation of Rossby waves. The Plumb WAF was proposed for analyzing the three-dimensional propagation characteristics of stationary Rossby waves (Plumb 1985). Then the T-N WAF proposed by Takaya and Nakamura (2001) has a larger meridional component than the Plumb WAF. Under quasi-geostrophic conditions, the T-N WAF is appropriate for analyzing Rossby wave disturbance of the westerlies in a zonally asymmetric flow. Therefore, they are widely used in climate monitoring and weather diagnosis. The horizontal component of T-N WAF is:

$$W = \frac{pcos\varphi}{2|U|} \left( \frac{U}{a^2cos^2\varphi} \left[ \left( \frac{\partial\psi'}{\partial\lambda} \right)^2 - \psi' \frac{\partial^2\psi'}{\partial\lambda^2} \right] + \frac{V}{a^2cos\varphi} \left[ \frac{\partial\psi'}{\partial\lambda} \frac{\partial\psi'}{\partial\varphi} - \psi' \frac{\partial^2\psi'}{\partial\lambda\partial\varphi} \right] \right. \\ \left. \frac{U}{a^2cos\varphi} \left[ \frac{\partial\psi'}{\partial\lambda} \frac{\partial\psi'}{\partial\varphi} - \psi' \frac{\partial^2\psi'}{\partial\lambda\partial\varphi} \right] + \frac{V}{a^2} \left[ \left( \frac{\partial\psi'}{\partial\varphi} \right)^2 - \psi' \frac{\partial^2\psi'}{\partial\varphi^2} \right] \right) \quad (1)$$

with  $\psi = \frac{\Phi}{f}$ ,

Variables with superscript “'” represent perturbations.  $\Phi$  represents geopotential.  $\varphi$  and  $\lambda$  represent latitude and

longitude, respectively.  $f$  represents the Coriolis parameter.  $a$  and  $\Omega$  represent the Earth's radius and rotation rate, respectively.  $U$  and  $V$  represent the multiyear average climatic fields of basic flow. Using this method, the propagation characteristics of Rossby waves that may exist during the Arctic sea ice process affecting the BSISO were analysed.

When analysing the possible impact of SST anomaly (SSTA) near Japan on the phases of BSISO to reduce the potential interference of El Niño decaying years, this study adopts the formula proposed by Ashok et al. (2003) to remove the signal of Niño3.4 from the relevant variables. The expression is:

$$I_{RB} = I_B - r(I_B, I_A)O\tilde{I}_A \quad (2)$$

$I_A$  is the Niño3.4 index and  $\tilde{I}_A$  is the normalised  $I_A$ .  $I_B$  is the regional variables, and  $O$  is the standard deviation of  $I_B$ .  $r(I_B, I_A)$  denotes the correlation coefficient between  $I_A$  and  $I_B$ .  $I_{RB}$  represents the variables without the Niño3.4 signal.

In addition, statistical methods such as composite analysis, regression analysis, and correlation analysis were adopted, and their results were examined for confidence levels using the Student's  $t$ -test.

### 3 Results

#### 3.1 Relationship between Arctic SIC and BSISO phases

Based on the duration of the ISO, the BSISO is divided into two components: BSISO1 (30–60 days) and BSISO2 (10–30 days). These components consist of eight phases that depict the eastward or northward as well as northwestward or northeastward propagation of intraseasonal variability in the ASM region (Lee et al. 2013). First, this section used the BSISO1 and BSISO2 indices to analyse their characteristics

in summer and identify the relationship between the BSISO components and the preceding Arctic sea ice.

Figure 1 shows the annual frequency distribution of each phase for BSISO1 and BSISO2 during JJA. Notably, both components exhibited significant interannual variation. The frequency range for all phases of BSISO1 spans 1 to 31 days, with phase 2 showing the highest variance of 51.26 day<sup>2</sup> (ranging from 1 to 31 days) and phase 1 exhibiting the lowest variance of 22.08 day<sup>2</sup> (ranging from 2 to 19 days). Similarly, for BSISO2, the frequency range for all phases covers 1 to 28 days, with phase 2 having the highest variance of 40.45 day<sup>2</sup> (ranging from 4 to 28 days) and phase 5 showing the lowest variance of 17.29 day<sup>2</sup> (ranging from 2 to 21 days). Based on this comparison, it can be inferred that the interannual variability in frequency is generally more pronounced in BSISO1 than in BSISO2.

Additionally, Fig. 1c shows each phase's 30-year average frequency distribution for BSISO1 and BSISO2 during JJA. Phase 2 and 3 of BSISO1 exhibited relatively high frequencies, averaging 13.7 days and 13.1 days per JJA, respectively, with associated convection primarily located over the equatorial Indian Ocean. In contrast, phase 6 of BSISO2 had the highest frequency, averaging 13 days per JJA, and was associated with convection in the Bay of Bengal-East Asia-western North Pacific region.

We explored the potential relationship between Arctic sea ice from winter (December to February, DJF) to spring (March to May, MAM) and the BSISO during the following JJA period, considering the statistical characteristics of the BSISO obtained above. This is due to the pronounced interannual and seasonal variations of Arctic sea ice, which change relatively slowly compared to the atmosphere, leading to a lag effect.

Figure 2 shows the regressed Arctic SIC in DJF and MAM for the frequency-time series in each phase of the JJA BSISO1. In DJF, the SIC north of the East Siberian-Beaufort Sea (hereafter, the ESBS) significantly correlated with the frequency of phases 3 and 7 of the BSISO1. A negative SIC



**Fig. 1** The time series of frequency in each phase of **a** BSISO1 and **b** BSISO2 during JJA from 1991 to 2020; **c** the 30-year average frequency in each phase of BSISO during JJA (unit: day)

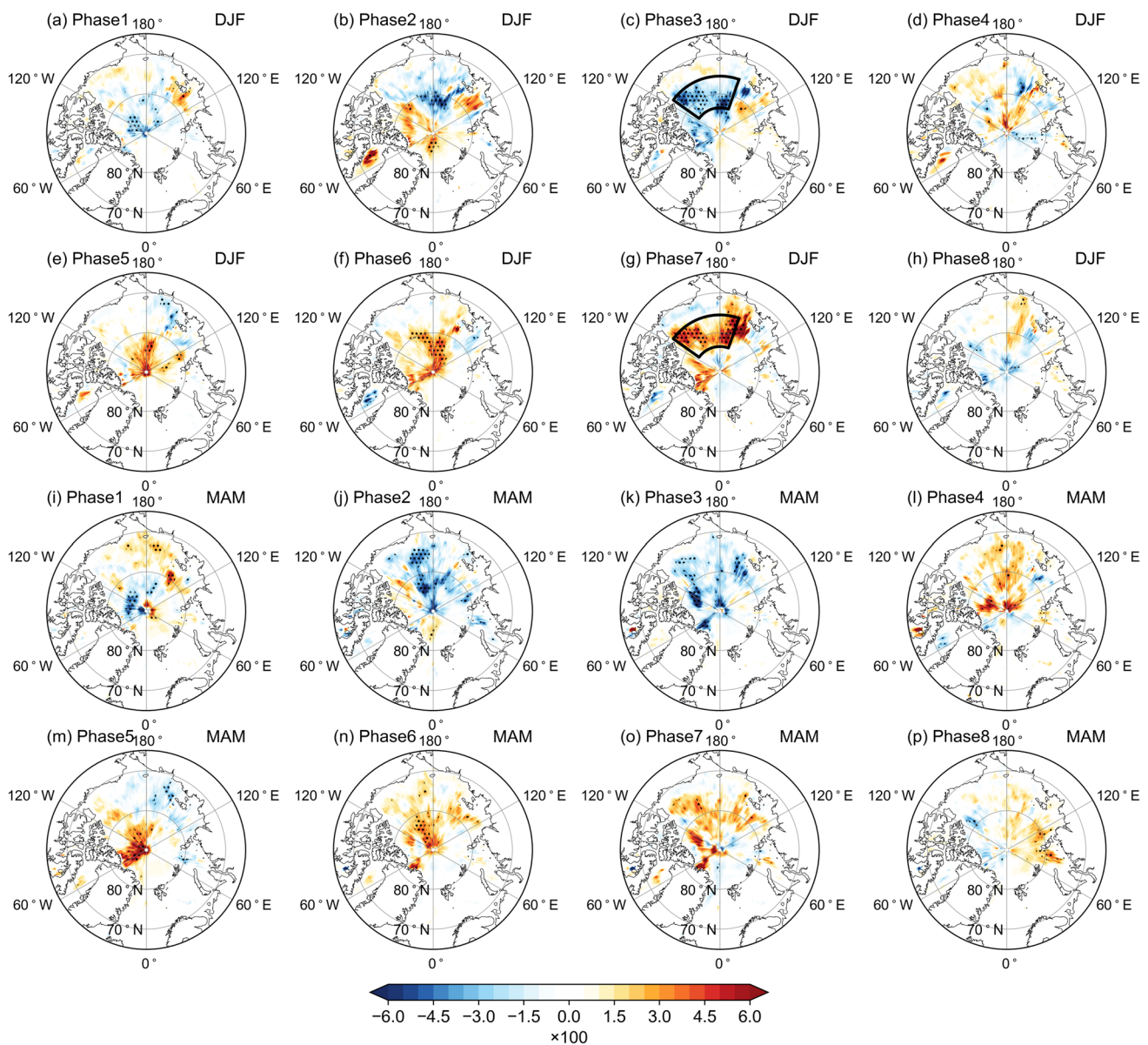


**Fig. 2** Regressed SIC in the previous (a–h) DJF and (i–p) MAM to the frequency-time series in each phase of JJA BSISO1. The black boxes in panels (c) and (g) represent the ESBS. At the same time, the

dots denote the regions where the regressions show statistical significance above the 90% confidence level, determined using the Student’s *t*-test

anomaly in this region corresponded to more days in phase 3 (Fig. 2c). In comparison, it corresponded to more days in phase 7 for positive SIC anomaly years (Fig. 2g). Compared with the ESBS, the relationships between SIC in other regions and the frequency in each phase of the BSISO were not significant. Therefore, we designated the ESBS as a key region for the impact of the DJF and MAM Arctic sea ice on the JJA BSISO1, with a specific range (160°E–125°W, 75–84°N) (black boxes in Fig. 2c, g). Figure 2i–p showed the relationship between the MAM SIC and BSISO1. The signal in the ESBS was a little weaker during MAM than during DJF, but no significant signals were found in the other

regions. Furthermore, we conducted a regression analysis to examine the relationship between the Arctic SIC anomaly during DJF and MAM and the frequency time series of each phase in the BSISO2. The results showed significant regions in phases 2, 4, 6, and 7 of the BSISO1 (Fig. 3b, d, f, and g), as well as phase 2 of the BSISO2 (Fig. 3j). Notably, Laptev Sea, exhibited a significant negative correlation with the phase 2 (Fig. 3b). In contrast, the northern region of the New Siberian Islands showed a positive correlation with the phase 4 (Fig. 3d). However, compared to the results for BSISO1, these regions displayed a scattered spatial distribution and a narrower scope (Fig. 3b, d, f, g, and j), indicating a stronger

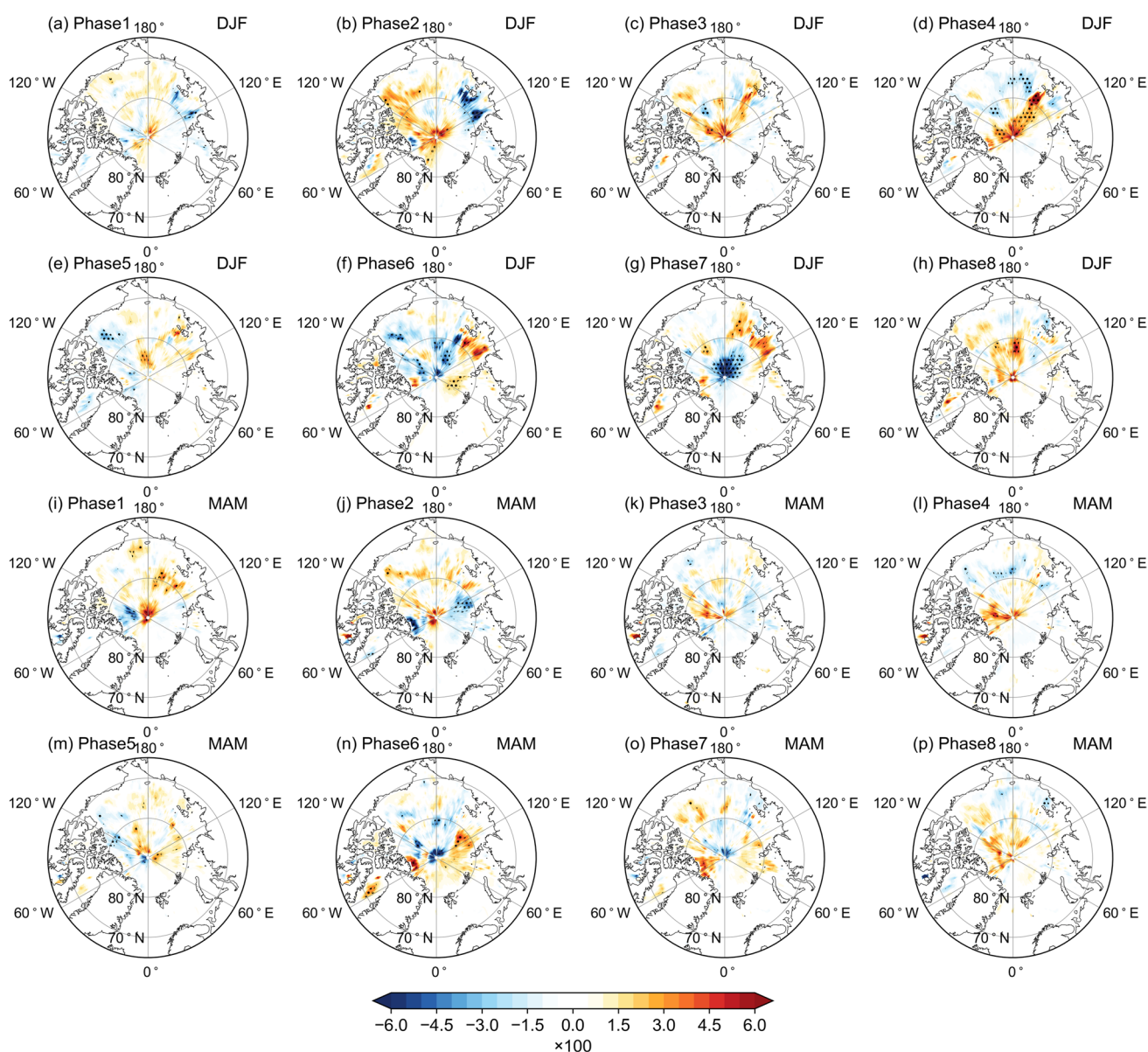


**Fig. 3** As in Fig. 2, but for BSISO2

and more apparent relationship between the DJF and MAM SIC and the subsequent JJA BSISO1.

To further analyse the two crucial phases of BSISO1 and the SIC in the ESBS, we composited the 850 hPa horizontal wind and OLR corresponding to phases 3 and 7 based on the daily BSISO1 index in JJA. In phase 3, the convection centre was located over the tropical Indian Ocean and the Maritime Continent, accompanied by an anomalous low-level cyclone. Conversely, convection was suppressed over the South China Sea-western North Pacific, with an anomalous low-level anticyclone (Fig. 4a). The spatial distribution of phase 7 exhibited the opposite pattern. Convection was active over the South China Sea-western North Pacific, accompanied by

an anomalous cyclone in the lower troposphere. Meanwhile, convective suppression and an anomalous anticyclone were observed over the tropical Indian Ocean and the Maritime Continent (Fig. 4b). These findings aligned with the results reported by Lee et al. (2013).

Additionally, we calculated and standardized the regional average SIC as a new index representing the ESBS in winter and the subsequent spring (Fig. 4c). It demonstrated that the ESBS's SIC indices in DJF and MAM display obvious interannual variability, with a statistically significant correlation coefficient of 0.68 above the 99% confidence level; this indicates a clear continuity in SIC changes from DJF to MAM in the ESBS. Therefore,

**Fig. 4** Compositing 850 hPa horizontal wind (vector, unit: m/s) and OLR (shaded, unit:  $W/m^2$ ) corresponding to **a** phase 3 and **b** phase 7 based on the daily BSISO1 index in JJA; **c** the standardized regional average SIC indices of DJF and MAM. The solid grey lines in panel (c) denotes  $\pm 0.8$  standard deviations

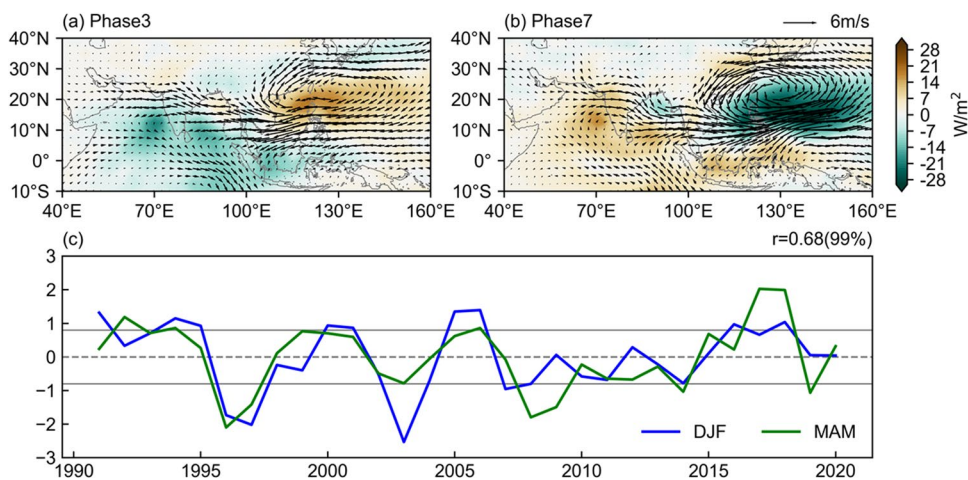


**Table 1** Correlation coefficients between the DJF SIC index and the frequency-time series in each BSISO phase

	Phase 1	Phase 2	Phase 3	Phase 4	Phase 5	Phase 6	Phase 7	Phase 8
BSISO1	-0.12	-0.18	<b>-0.41*</b>	-0.03	0.10	0.25	<b>0.39*</b>	0.03
BSISO2	0.08	0.13	-0.02	-0.20	-0.10	-0.15	0.03	0.15

\* and the bold value denote the significant correlation at a 95% confidence level

considering the stronger relationship between DJF SIC and BSISO1 in Fig. 2, we utilise the DJF SIC index to measure Arctic sea ice in the subsequent analysis.

The correlation coefficients between the DJF SIC index and the frequency-time series in each phase of the BSISO were calculated. As shown in Table 1, for BSISO1, the correlation coefficient between the SIC index and the time series of phase 3 was -0.41, and phase 7 was 0.39, which was statistically significant above the 95% confidence level. Except for these, the correlations between the SIC index and the time series of the other phases of the BSISO1 and phases of the BSISO2 were not significant. The above results correspond to Figs. 2 and 3, suggesting a negative (positive) correlation between the DJF SIC in the ESBS and the frequency in phase 3 (7) of the JJA BSISO1. That is, when the DJF SIC in the ESBS region was anomalously high, then phases 3 (7) of BSISO1 were anomalously decreased (increased) in the following JJA.

Using the DJF SIC index, we classified the high- or low-SIC years of the ESBS based on  $\pm 0.8$  standard deviation. There were nine high-SIC years: 1991 (the corresponding winter was from December 1990 to February 1991), 1994, 1995, 2000, 2001, 2005, 2006, 2016, and 2018. Low-SIC years were 1996, 1997, 2003, 2007, and 2008. Table 2 showed that phase 3 of BSISO1 had a climatology of 13.1 days, an average of 9.9 days in a high-SIC year, and 16.6 days in a low-SIC year. For phase 7, the above values were 10.3, 15.1, and 7.4 days, respectively. The difference in frequencies between high- or low-SIC

years and normal years was the largest in these two phases compared to the other phases.

### 3.2 Circulation and water vapour anomalies related to BSISO1

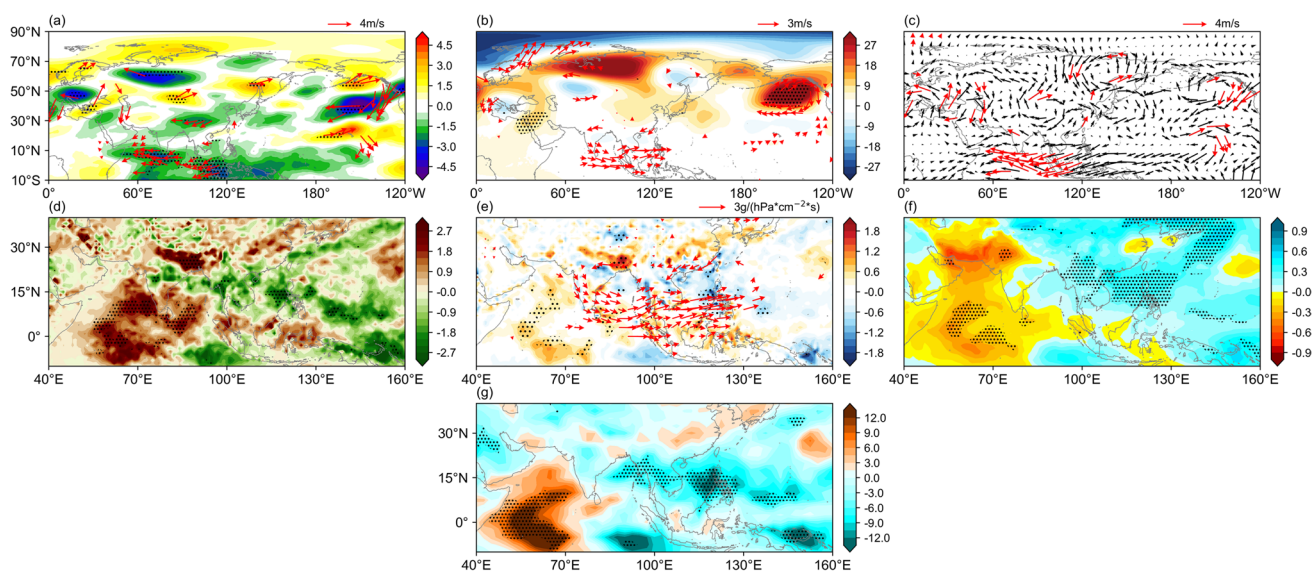
The development and propagation of the BSISO are closely related to large-scale circulation and water vapour. Therefore, this section first exhibited summer background fields in typical SIC years and analysed the physical conditions favouring phases 3/7 of the BSISO1.

Figure 5 shows the composited differences of atmospheric circulation and water vapour anomalies, which may

**Table 2** The average frequency in each phase of BSISO1 in the high-/low-/normal SIC years (unit: day)

	High-SIC years	Low-SIC years	Normal years
Phase 1	8.0 (-0.7)	10.6 (+1.9)	8.7
Phase 2	10.9 (-2.8)	16.2 (+2.5)	13.7
Phase 3	<b>9.9 (-3.2)</b>	<b>16.6 (+3.5)</b>	13.1
Phase 4	11.2 (-0.9)	11.2 (-0.9)	12.1
Phase 5	12.4 (-0.1)	11.8 (-0.7)	12.5
Phase 6	11.9 (+1.8)	8.6 (-1.5)	10.1
Phase 7	<b>15.1 (+4.8)</b>	<b>7.4 (-2.9)</b>	10.3
Phase 8	12.4 (+0.9)	9.6 (-1.9)	11.5

The values in brackets denote the difference between the high-/low-SIC years and normal years and the bold value denote the extremums



**Fig. 5** Composed differences of **a** 200 hPa horizontal wind (vector, unit: m/s) and zonal wind (shaded, unit: m/s), **b** 500 hPa horizontal wind (vector, unit: m/s) and geopotential height (shaded, unit: gpm), **c** vertical wind shear between 200 and 850 hPa (unit: m/s), **d** 500 hPa vertical velocity (unit: pascal/s), **e** average water vapour

flux (vector, unit:  $\text{g}/(\text{hPa}\cdot\text{cm}^2\cdot\text{s})$ ) and its divergence (shaded, unit:  $\text{g}/(\text{hPa}\cdot\text{cm}\cdot\text{s})$ ) among 1000 to 600 hPa, **f** specific humidity among 1000 to 600 hPa (unit:  $\text{g}/\text{kg}$ ) in JJA. The red vectors and the dots denote the regions where the composites are statistically significant above 95% confidence level based on the Student's *t*-test

be related to phases 3/7 of BSISO1 in the high- and low-SIC years. Compared with low-SIC years, it is observed that during the summer of high-SIC years, significant anomalous easterly flow occurred in the lower level over the region from the tropical Indian Ocean to the Marine Continent. At the same time, anomalous westerly winds in the upper level over the region from the southern Indian Peninsula to the Philippine Islands resulted in anomalous vertical easterly shear (Fig. 5a–c). Notably, the northeastern wind shear was more pronounced from the Bay of Bengal to the east of the Philippine Islands. Previous studies have highlighted the influence of vertical easterly and northerly wind shear on the propagation of the BSISO (Wang and Xie 1996; Xie and Wang 1996; Wang et al. 2006; Bellon and Sobel 2008; Dixit and Srinivasan 2011). Therefore, the easterly/northeasterly shear observed in the tropical Indian Ocean and western Maritime Continent may promote the northwestward propagation of convection towards the Pacific.

Moreover, Fig. 5d revealed a significant descending motion over the western tropical Indian Ocean and an ascending motion over the South China Sea and western North Pacific. This condition, combined with anomalous easterly winds in the upper layers and anomalous westerly winds in the lower layers between these regions, led to an enhanced Walker circulation forming over the ASM region. The upward branch of the Walker cell, situated over the western Pacific Ocean, provided favourable conditions for convection over the western Pacific, corresponding to the higher frequency of phase 7 in the BSISO1.

In addition to the large-scale circulation, water vapour also plays a significant role in the propagation of the BSISO. Figure 5e revealed important water vapour characteristics in the region (70–130°E, 0°–15°N). There was notable west-to-east water vapour transport in the middle and lower levels, with a small portion reaching the Bay of Bengal. Simultaneously, water vapour diverged in the western equatorial Indian Ocean, while convergence was observed in the South China Sea and the Philippine Sea. Consequently, specific humidity among the middle and lower layers was considerably higher from the Indo-China Peninsula to the Philippine Sea, creating a zonal humidity gradient with the western tropical Indian Ocean (Fig. 5f). Previous studies have proved that anomalous moist static energy can influence the development and propagation of the BSISO, and water vapour transport and humidity variability contribute to the accumulation or consumption of moist static energy (Deng and Li 2016; Liu and Wang 2016). Therefore, the water vapour budget and specific humidity anomalies in the middle and lower levels shown in Fig. 5e, f indicated that moist static energy tended to accumulate over the Bay of Bengal, South China Sea, and the Philippine Sea, facilitating the eastward spread and development of convection along this trajectory.

These dynamic and thermal conditions were favourable for the frequency of phase 7 in the BSISO1. By comparing Fig. 5g and 4b, it is easy to find that they have similar convection regions; this further proved that compared to low-SIC years, high-SIC years have active convection over the Philippine Sea and the South China Sea, corresponding to the characteristics of the phase 7 of BSISO1.



### 3.3 Possible mechanism of Arctic SIC impact on BSISO1

This section will explain the impact of the DJF Arctic SIC anomaly on the summer BSISO1. Two important questions arise in understanding the relationship between the Arctic SIC and BSISO: Firstly, considering the vast distance between the ESBS and the ASM region, how the Arctic sea ice anomaly signal is transmitted to low-latitude regions needs to be clarified. Secondly, it is known from previous studies that the Arctic sea ice anomalies can affect meteorological elements for several months, lasting up to four months (Walsh 1980). Based on the observed facts of the significant negative (positive) correlation between the DJF SIC of the ESBS and the frequency of phase 3 (7) of the JJA BSISO1, it is crucial to understand the persistence of winter signals and their continuity across seasons until summer.

Additionally, the above findings show that the SIC of the ESBS in DJF mainly affected phases 3 and 7 of the BSISO1 in JJA, corresponding to suppressed or active convection around the Philippine Sea, respectively. Consequently, this section investigated the mechanisms through which SIC anomalies in the ESBS modulate the variability of atmospheric variables over the Philippine Sea, resulting in anomalous changes in the frequency of the BSISO phases.

#### 3.3.1 Response of the Western North Pacific SST to SIC anomaly

The mid-latitude region of the Northern Hemisphere connects the Arctic and tropics, often serving as an intermediary in their interaction. In addition, due to the large thermal capacity of seawater, the ocean has better memory than the atmosphere. Previous studies have also shown that SST does play a crucial role in the cross-seasonal impact of Arctic sea ice on regions outside the polar (Chen et al. 2023a; Fu et al. 2021; Kim et al. 2020). Therefore, we first analyzed the response of the mid-latitude North Pacific to the ESBS SIC anomaly.

Figure 6 showed the composite difference in the atmospheric variable fields from DJF to JJA. The AL gradually deepened from DJF to MAM, peaked between March and May (Fig. 6d, k) and rapidly weakened from June (Fig. 6e, l). The wind field also exhibited a strengthening and weakening process of the cyclonic circulation anomaly synchronised with the AL. Since late winter and early spring, enhanced high pressure has controlled the south of the AL. It is accompanied by an anomalous anticyclone (Fig. 6b, i), forming a meridional dipole distribution with the strengthened AL and anomalous cyclonic circulation over the Bering Sea. The anomalous anticyclone also weakened and moved eastward after June (Fig. 6e, l).

In addition to the large-scale circulation, the variation in SST in the North Pacific was also shown (Fig. 6o–u).

From winter to early spring, the SST in the Okhotsk Sea was significantly lower, whereas that in the subtropical Central Pacific was significantly higher (Fig. 6o and p). At that time, there was a positive SSTA east of Japan and a negative anomaly west. According to Fig. 6q–t, the positive SSTA east of Japan became significant and expanded gradually. The SST west of Japan also began to shift from a negative to a positive anomaly at the turn of spring and summer, ultimately leading to significant sea basin warming near Japan during JJA (Fig. 6u). Compared to the evolution of the dipole circulation anomaly, it was observed that the formation of SST positive anomaly near Japan lagged behind it. The three-month running average of the variable field regressed against the DJF SIC index (Figure not shown). It revealed the dipole structure and warming in the sea basin near Japan although the significance level was slightly lower than that in Fig. 6o–u.

Hence, it is necessary to establish a relationship between the wind and surface pressure patterns over the North Pacific and the SSTA around Japan corresponding to the typical SIC years. Compared to the low-SIC years, a gradually strengthened cyclone-anticyclone structure was observed in the high-SIC years. Then the northeasterly on the western-side of the anomalous cyclone and the southwesterly on the northwesternside of the anomalous anticyclone converged at about 50° N in lower levels.

In this case, the northeasterly transported dry and cold air from higher latitudes to the region near the Kamchatka Peninsula. Conversely, the southwesterly transported moist and warm air from lower latitudes to the region near Japan. The former led to increased upward sensible and latent heat fluxes from the sea surface, while the latter induced downward fluxes. Additionally, the wind stress intensified the convergence of the Kuroshio current and the Oyashio current near approximately 50° N. This convergence caused of warm and cold seawater accumulation in the vicinity of Japan and the Kamchatka Peninsula, thus amplifying the meridional SST gradient. Accordingly, warm and cold seawater heated and cooled the local lower atmosphere to increase the meridional air temperature gradient, enhancing the atmospheric baroclinicity.

Therefore, under the combined effect of sea surface heat flux and wind stress, during spring to early summer, the SST near Japan showed a significant positive anomaly, whereas that near the Kamchatka Peninsula showed a significant negative anomaly. Close to the end of summer, the significant negative SSTA gradually weakened, possibly affected by southerly winds west of the anomalous anticyclone moving eastward. However, the positive SSTA can remain throughout summer, which may be attributed to local cloud-radiation-SST positive feedback. The southwesterly winds of anomalous anticyclone resulted in the initial positive SSTA by increased upward heat fluxes and the accumulation of warm sea water at the turn of

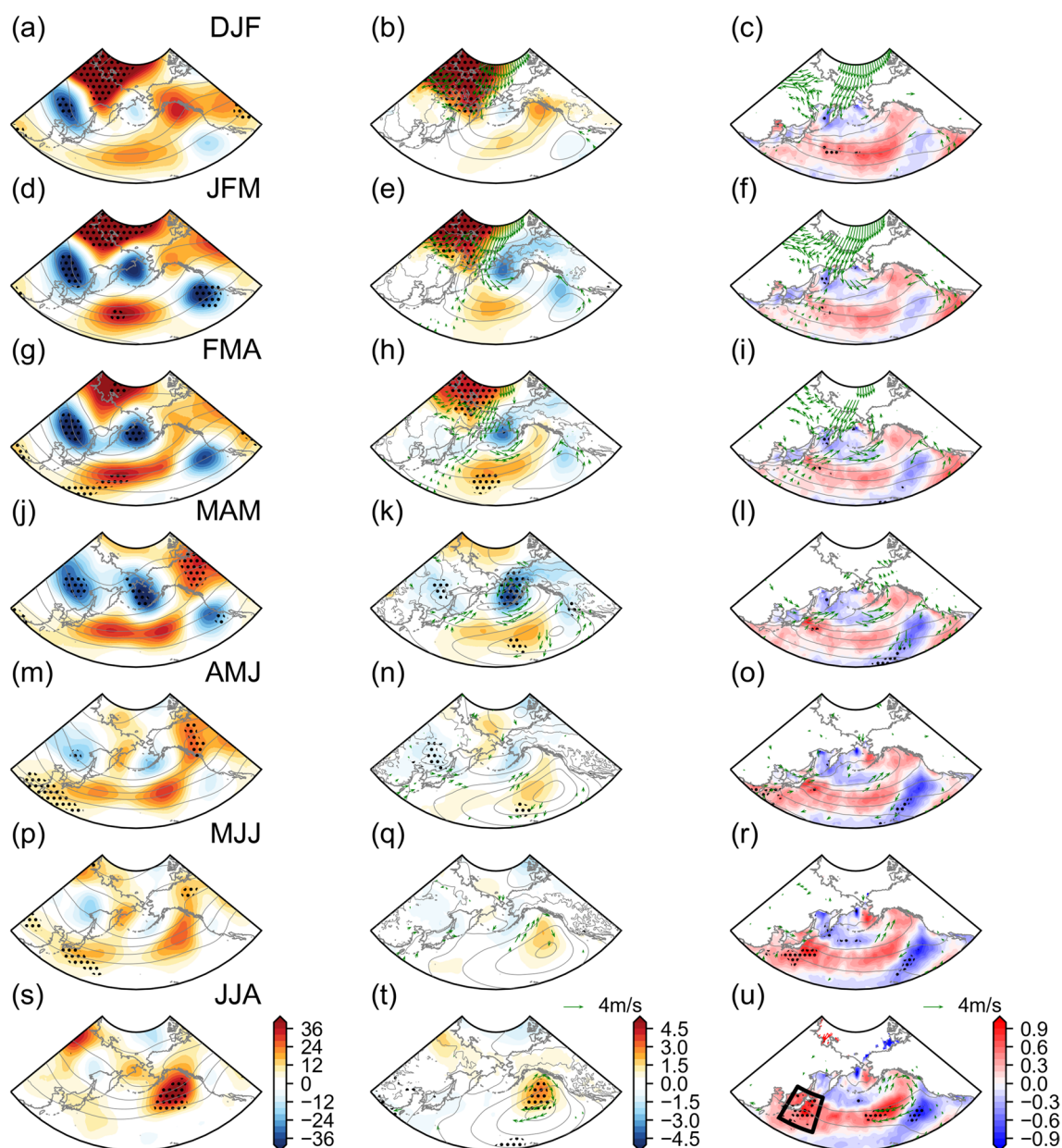


**Fig. 6** Composite difference of three-month sliding averaged (a, d, g, j, m, p and s) 500 hPa geopotential height (shaded, unit: gpm) (left column) (b, e, h, k, n, q and t) 925 hPa horizontal wind (vector, unit: m/s) and sea level pressure (shaded, unit: hPa) (middle column) (c, f, i, l, o, r and u) 850 hPa horizontal wind (vector, unit: m/s) and SST (shaded, unit: °C) (right column) from December to August of the

following year. The black box in panel (u) denotes the Japan region of SST. The green vectors and the dots denote the regions where the composites are statistically significant above the 95% confidence level based on the Student's *t*-test. The grey isoclines denote the climatology of 500 hPa geopotential height (left column), sea level pressure (middle column) and SST (right column)

spring and summer. It increased the instability of the lower troposphere, and the formation of low clouds was suppressed. Then, the anomalous anticyclone moved eastward and weakened. However, the anomalously reduced low clouds allowed more shortwave radiation to reach and heat the sea surface, which enhanced the boundary layer's stability and reduced the low clouds. Through this positive feedback mechanism, the positive SSTA near Japan was maintained.

The difference between high- and low-SIC years in the North Pacific is primarily evident in the dipole distribution of circulation anomalies over the Bering Sea and its south from winter to spring and the elevated SST near Japan during summer. Understanding the mechanisms through which the SIC anomaly in the ESBS influences the formation of the dipole structure in wind and geopotential height anomalies is essential. Additionally, whether the warm SST near

Japan will impact the convective activity associated with BSISO1 on its southern side is also a question that needs to be answered.

### 3.3.2 Response of mid-to-high-latitude circulation over the North Pacific to SIC anomaly

The anomaly in Arctic sea ice can potentially influence the local atmosphere by altering the sea surface heat flux. This signal can then propagate to the lower latitudes through processes such as atmospheric teleconnection and air-sea interaction, thereby impacting weather and climate patterns in the high, middle, and even low latitudes beyond the Arctic region (Honda et al. 2009; Fu et al. 2021; Duan et al. 2022). Hence, to investigate the mechanism through which the ESBS SIC affects circulation via local thermal processes, we have presented the composite difference of the three-month sliding averaged sensible heat flux between the high- and low-SIC years (Fig. 7). During winter and early spring, the sensible heat flux exhibited a negative anomaly, primarily concentrated in the key SIC region (Fig. 7a–c); this suggested that the significantly elevated SIC reduced heat transfer from the ocean to the atmosphere, consequently contributing to negative temperature anomalies and anticyclonic circulation patterns over it.

Many studies have revealed that thermal anomalies of the underlying surface induced by Arctic sea ice anomaly play an important role in triggering quasi-stationary Rossby waves, of which the downstream dispersion effect can provide disturbance energy for weather and climate change (Honda et al. 2009; Wu et al. 2013; Duan et al. 2022). To investigate how the atmospheric changes related to the ESBS SIC anomaly affect the circulation outside the Arctic, the T-N WAF was calculated to exhibit the related propagation of Rossby waves.

From January to March, the WAF can be seen from northeast to southwest between the ESBS SIC region and the Bering Sea at 700 hPa and 850 hPa, and the WAF converged

over the Bering Sea. The wave energy gathered here was conducive to developing or maintaining local disturbances corresponding to the negative anomaly of the quasi-geostrophic stream function and contributed to the enhancement of the AL (Fig. 8b, e). After reaching the Bering Sea, the WAF originating from the ESBS region failed to propagate southward to lower latitudes. From February, the WAF anomaly weakened, especially at 700 hPa (Fig. 8c). This also corresponds to the result that the sensible heat flux anomaly in the ESBS SIC region in the MAM was weaker than before (Fig. 7d). Some studies have suggested that the enhanced AL in early spring can induce an anomalous anticyclone to the south through the feedback of the synoptic-scale eddy-to-mean-flow energy flux and associated vorticity transportation over the North Pacific (Chen et al. 2020, 2023b, c). It is conducive to the forming the meridional dipole structure as shown in Fig. 6.

### 3.3.3 Impact of positive SSTA on the convection over the Philippine Sea

In this section, we analysed the effect of the positive SSTA near Japan on convection over the Philippine Sea during the same summer. First, an SST index defined as the summer SSTA averaged in the region near Japan ( $132^{\circ}$ – $154^{\circ}$ E,  $27^{\circ}$ – $47^{\circ}$ N), as shown by the black box in Fig. 6u, to investigate its potential impact on the convection over the Philippine Sea. Considering the characteristics similar to El Niño decaying years in the tropical Pacific in the previous composite analysis of SST (Fig. 6o–u), as well as the tropical atmosphere response closely related to the tropical ISO (Hu et al. 2022), the Niño-3.4 signal of the previous winter was removed from the variable fields using Eq. (2) to reduce its interference. The regression analysis results before and after removing the Niño 3.4 signal were roughly the same (figure not shown), indicating that the impact of the positive SSTA near Japan was independent of the El Niño event.

The turbulent heat flux (the sum of the latent and sensible heat fluxes) is critical physical variable for measuring air-sea

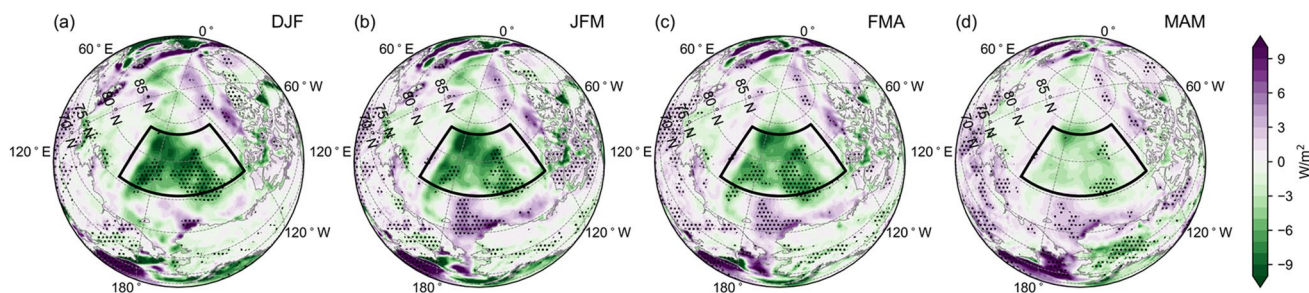


**Fig. 7** Composite difference of (a–d) three-month sliding averaged sensible heat flux between high- and low-SIC years from December to March of the following year (unit:  $\text{W}/\text{m}^2$ ). The black boxes in all

panels denote the key region of SIC. Dots denote the regions where the composites are statistically significant above the 90% confidence level based on the Student's *t*-test

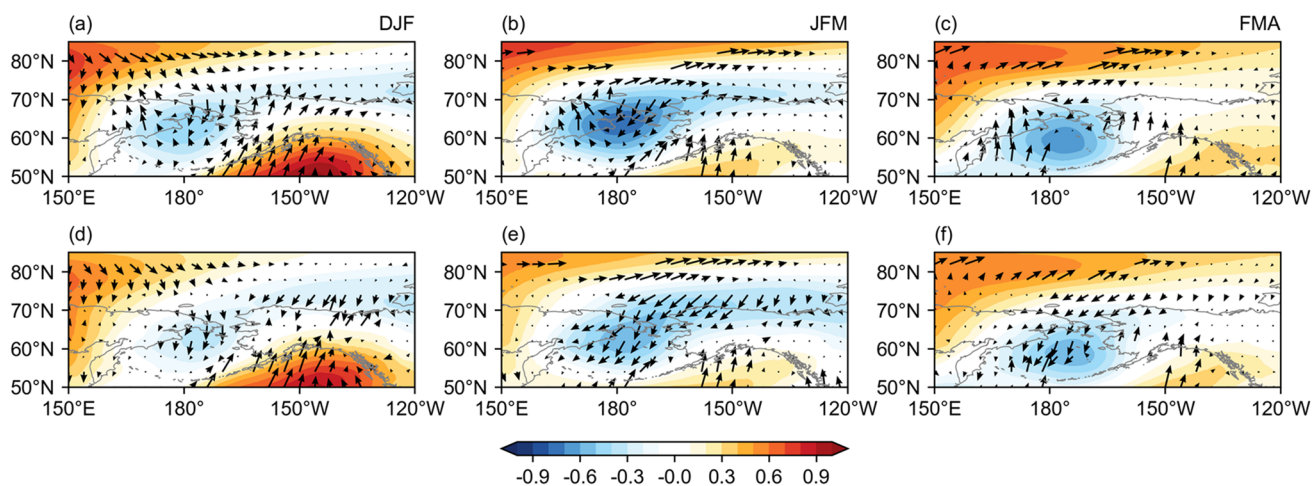
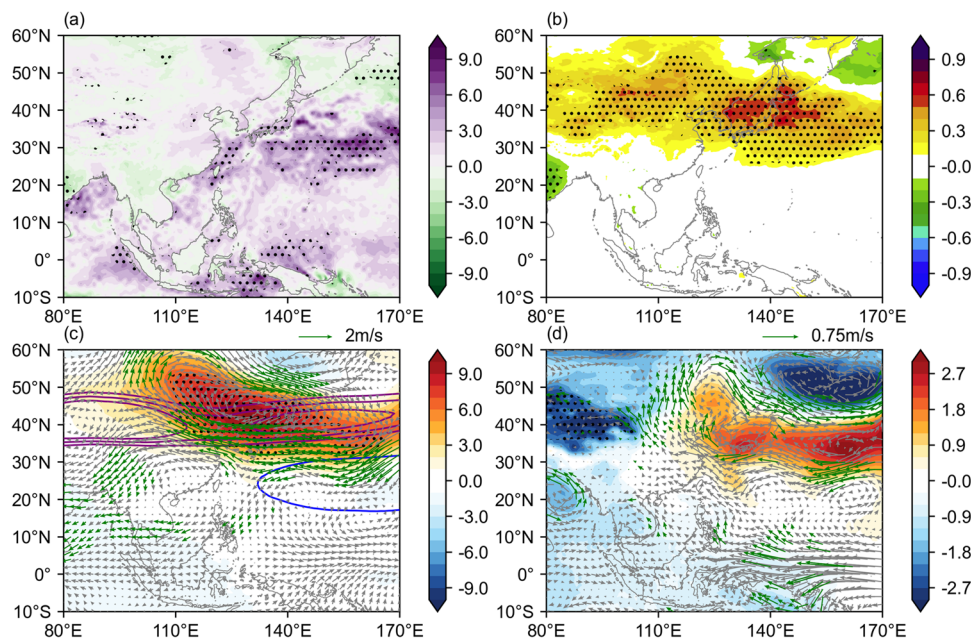


**Fig. 8** Regressed three-month sliding averaged (a–c) 700 hPa and (d–f) 850 hPa WAF (vector, unit:  $\text{m}^2/\text{s}^2$ ) and quasi-geostrophic stream function (shaded, unit:  $10^6\text{m}^2/\text{s}$ ). The black boxes in all panels denote the ESBS of SIC with respect to the DJF SIC index

interaction in the middle and low latitudes (Fig. 9a). A significant upward turbulent heat flux anomaly was observed over the western North Pacific, particularly above the sea surface east of Japan. This indicates that the ocean transports heat to the atmosphere in these regions. The regressed 2 m temperature in JJA also revealed that the temperature near Japan was significantly higher, and with two positive anomaly centres over the Sea of Japan and the sea area east of Japan (Fig. 9b). Atmospheric warming induced by SST heating created favourable conditions for circulation anomalies. Considering the responses of the mid-latitude upper troposphere to the ocean surface heat flux anomaly (Qian et al. 2023), we further analysed the changes in geopotential

height and horizontal wind over the western North Pacific related to SST warming near Japan. As shown in Fig. 9c, a significant positive geopotential height anomaly accompanied by an anomalous anticyclone was observed over the region from Lake Baikal to the western North Pacific, with its centre located over the Northeast China Plain. In comparison to the climatology of the western Pacific subtropical high (WPSH) (as defined by Guan et al. (2019)) and the subtropical westerly jet (SWJ), the positive geopotential height anomaly and the westerly to the north of the anomalous anticyclone, extending from Lake Baikal to the western North Pacific, reinforced and pushed the WPSH and SWJ northward, respectively. The position of the positive

**Fig. 9** Regressed a turbulence heat flux (unit:  $\text{W}/\text{m}^2$ ) b 2 m temperature (unit:  $^\circ\text{C}$ ) c 200 hPa horizontal wind (vector, unit:  $\text{m}/\text{s}$ ) and 500 hPa geopotential height (shaded, unit:  $\text{gpm}$ ) d 850 hPa horizontal wind (vector, unit:  $\text{m}/\text{s}$ ) and 925 hPa geopotential height (shaded, unit:  $\text{gpm}$ ) in the same JJA with respect to the SST index with the previous DJF Niño3.4 signal removed. The blue line and purple lines denote the climatology of the WPSH (5880  $\text{gpm}$ ) and the SWJ ( $u \geq 20 \text{ m/s}$ , interval of 2.5  $\text{m/s}$ ). The green vectors and the dots denote the regions where the regressions are statistically significant above the 95% confidence level based on the Student's  $t$ -test



geopotential height anomaly and anomalous anticyclone in the lower layer was more east and south than that in the upper layer, and the centre was located over southern Japan (Fig. 9d). These results suggested that through SST heating, the meridional air temperature gradient of the lower layer near Japan increased. According to the theory of thermal wind, the local atmospheric baroclinicity of the troposphere was enhanced, and the WPSH and SWJ were strengthened and moved northward.

At the same time, an anomaly cyclonic shear and the convergence of low-level winds occurred over the Philippine Sea to the south of Japan (Fig. 9d), and its association with the BSISO activity will be analysed in this section. For the upper troposphere, there was convergence over Japan in JJA. In contrast, the convergence over the Philippine Sea to the south was divergent (Fig. 10a). In the lower troposphere, there was a significant negative vorticity anomaly over the Korean Peninsula, Japan and its adjacent sea area, extending eastward to the western North Pacific. The Philippine Sea from 10°N to 30°N was dominated by the positive vorticity anomalies (Fig. 10b). The vertical velocity regression analysis also indicated that there was a descending motion near Japan in the middle troposphere. In contrast, the region from the South China Sea to the Philippine Sea was generally in ascending motion (Fig. 10c). Moreover, for phases 3 and 7 of BSISO1, their centres were mainly located from 115°E to 145°E. Therefore, the zonally averaged stream field within this range was also regressed with respect to the SST index (Fig. 10d).

According to Fig. 10d, there was a significant descending motion from the lower to upper levels in the mid-latitude region from approximately 45°N to 55°N. In the region

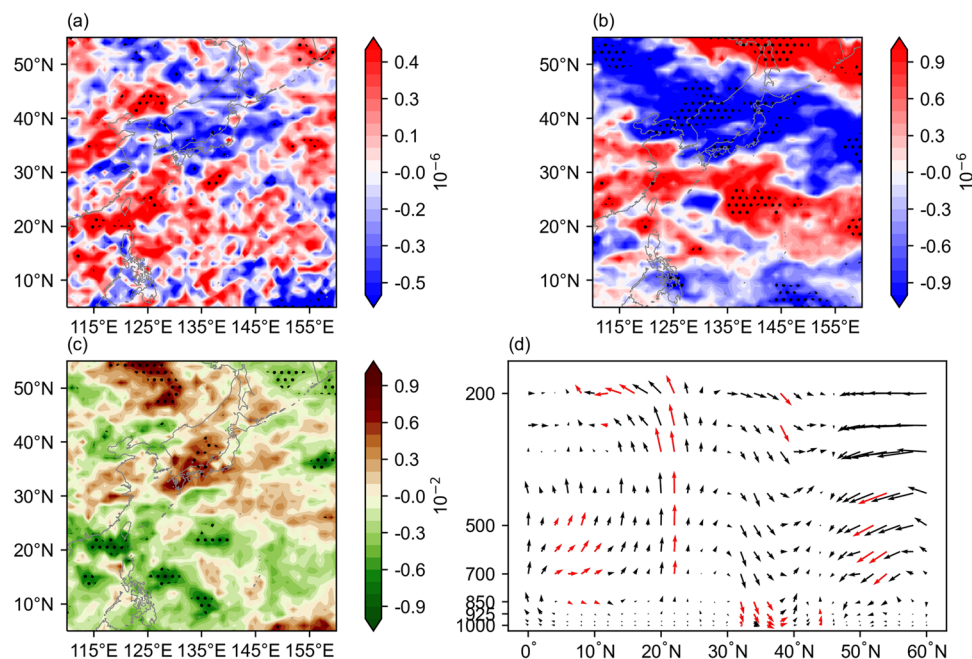
south of Japan, around 10°–25°N, the entire troposphere was in ascending motion, corresponding to the regions in which phase 3/7 of BSISO1 was located. The drifts flowed northward in the upper levels near 25°N to 45°N. It can be concluded that the positive SSTA triggered the northward movement and enhancement of the SWJ and WPSH. A negative vorticity anomaly was formed in the upper troposphere over Japan, into which drift flowed northward from the Philippine Sea, and the descending motion was enhanced. In addition, the northward flow can enhance the ascending motion over the Philippine Sea, accompanied by divergence in the upper level and a positive vorticity anomaly at the lower level, which corresponds to the anomaly cyclonic shear and convergence of low-level winds as shown in Fig. 9d. These provide potential conditions for active convection over the Philippine Sea and lead to a higher (lower) frequency of phase 7 (3) of the BSISO1.

## 4 Conclusion and discussion

Considering the critical role of Arctic sea ice in the global climate system and the significant impact of the Boreal Summer Intraseasonal Oscillation (BSISO) on weather and climate patterns, this study aimed to investigate the potential relationship between winter and spring Arctic sea ice conditions and the BSISO, as well as the underlying physical mechanisms.

The findings revealed a significant positive (negative) correlation between the winter Arctic sea ice in the key region (the Arctic Ocean north of the East Siberian-Beaufort

**Fig. 10** Regressed **a** 200 hPa divergence (unit:  $s^{-1}$ ) **b** 850 hPa vorticity (unit:  $s^{-1}$ ) **c** 500 hPa vertical velocity (unit: pascal/s) **d** zonal average (115°E to 145°E) stream field (unit: m/s) in the same JJA with respect to the SST index with the previous DJF Niño 3.4 signal removed. The red vectors and the dots denote the regions where the regressions are statistically significant above the 90% confidence level based on the Student's *t*-test



Sea, ESBS) and the frequency of phase 7 (3) of BSISO1 in the Asian Summer Monsoon (ASM) region ( $40^{\circ}$ – $160^{\circ}$  E,  $10^{\circ}$  S– $40^{\circ}$  N) during the subsequent summer season (JJA). However, no significant correlation was observed with BSISO2. These results suggested that a positive anomaly in the ESBS sea ice concentration (SIC) was associated with an increase in the frequency of BSISO1 phase 7. At the same time, a corresponding decrease was observed in phase 3. The characteristics of the background field in the ASM region during JJA for high- and low-SIC years were examined and compared. In high-SIC years, there was an easterly or northeasterly vertical wind shear to the west of the Arabian Peninsula.

Additionally, Walker circulation anomalies strengthen the sinking branch in the tropical Indian Ocean and the rising branch in the Western Pacific. Furthermore, a water vapour transport channel was observed from west to east in the mid-to-lower levels towards the Philippine Islands, which increased the humidity gradient between tropical Indian Ocean and western North Pacific. These dynamic and thermal conditions favoured the active convection over the Philippine Sea, corresponding to the higher (lower) frequency of phase 7 (3) of the BSISO1.

Further analyses showed the possible physical mechanisms of the impact of the previous winter Arctic SIC on the key phases of BSISO1 (Fig. 11). The high SIC in the ESBS during winter resulted in a downward sensible heat flux anomaly, cooling the local atmosphere and creating a negative geopotential height anomaly; this triggered WAF propagation from the key SIC regions to the Bering Sea, where its convergence facilitated the development and maintenance of local disturbances, strengthening the AL. In early spring, the intensified AL induced an anomalous

subtropical anticyclone through wave-mean flow interaction in the mid-latitude North Pacific, forming a meridional dipole distribution over the Bering Sea and its south. In the lower troposphere, the northeasterly winds to the west of the anomalous cyclone and the southwesterly winds in the northwestern part of the anomalous anticyclone converged around  $50^{\circ}$ N. The combined effect of sea surface heat fluxes and wind stress led to a significant positive anomaly in SST near Japan during MAM and JJA, driven by the local cloud-radiation-SST positive feedback. Conversely, the SST near the Kamchatka Peninsula exhibited a significant negative anomaly, potentially influenced by southerly winds and weakening in the late summer.

The impact of a positive sea surface temperature anomaly (SSTA) on the two key phases located over the Philippine Sea south of Japan is discussed. During the months of June, July, and August (JJA), the meridional temperature gradient in the lower atmosphere near Japan after increased as a result of being heated by SST. This led to the enhancement of baroclinicity in the troposphere. In the upper levels, significant positive geopotential heights and anticyclone anomalies were observed from Lake Baikal to the western North Pacific, along with the anomaly cyclonic shear and convergence of low-level winds over the Philippine Sea. These conditions favoured the strengthening and northward movement of the Western Pacific Subtropical High (WPSH) and the subtropical westerly jet (SWJ), while a negative vorticity anomaly formed in the upper troposphere over Japan. Northward flow, due to Ekman pumping, strengthened the descending motion over Japan and the ascending motion over the Philippine Sea. Additionally, divergent and positive vorticity anomalies were

**Fig. 11** The Schematic diagram shows how the DJF SIC of ESBS affects the frequency of phase 3 (7) of BSISO1 in JJA

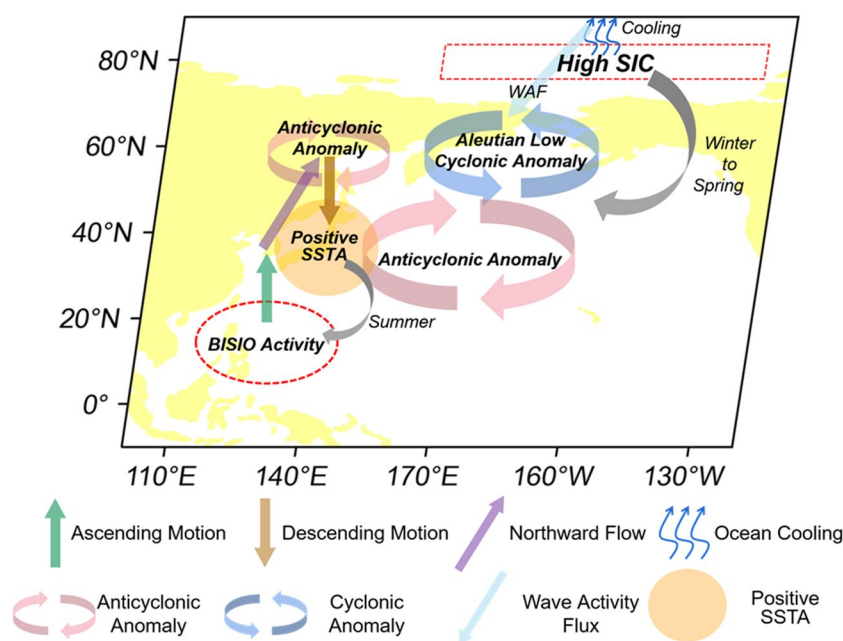
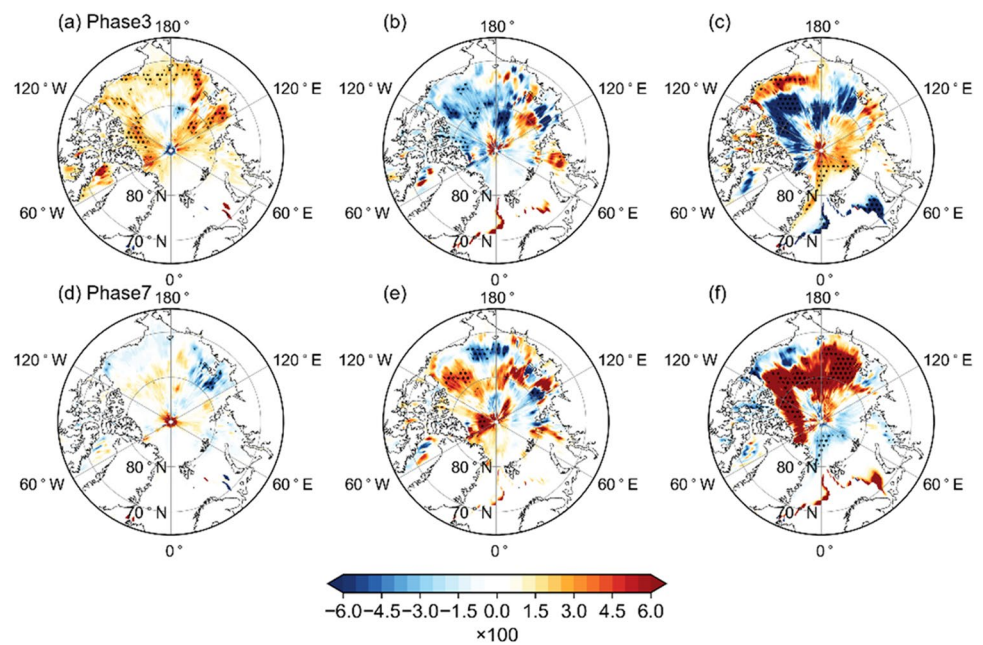


**Fig. 12** Regressed SIC in the previous DJF with respect to the time series of frequency in **a–c** phase 3 and **d–f** phase 7 of JJA BSISO1 in 1981–1998 (left column), 1999–2008 (middle column) and 2009–2020 (right column). The dots denote the regions where the regressions show statistical significance above the 90% confidence level, determined using the Student's t-test



present over the Philippine Sea at both upper and lower levels. These favourable conditions for convection supported the development and maintenance of the BSISO1 signal, ultimately resulting in a higher frequency of phase 7 and a lower frequency of phase 3.

Arctic sea ice has exhibited a melting rate several times higher since the late twentieth century. The interdecadal relationship between the Arctic sea ice and various weather and climate systems has received increasing attention in recent years. He et al. (2021) analysed the possible linkage between mid-to-high-latitude atmospheric circulation and Arctic sea ice loss in different locations and seasons and the associated impacts on winter climate on interdecadal timescales. The interdecadal variability of the relationship between Arctic sea ice and other weather and climate events, such as cold surges, summer wetting trend, atmospheric water vapor content in East Asia, and western China autumn rain, has been investigated (Sun et al. 2020; Yang et al. 2020; He et al. 2022; Zhou et al. 2023). The BSISO also shows characteristics of interdecadal variation (Kajikawa et al. 2009; Yamaura and Kajikawa 2017). Chen et al. (2023c) pointed out that enhancement of the mean circulation over the North Pacific led to an increase in the wave-mean flow interaction after the late 1990s, which may have contributed to the formation of the meridional dipole structure. However, it remains unclear whether the relationship between the two is stable on an interdecadal timescale.

Based on the interannual relationship between SIC and BSISO phase frequency that we have obtained, and considering the three sub-periods of BSISO mentioned in Yamaura and Kajikawa (2017), we regressed SIC in the previous DJF with respect to the time series of frequency in phase 3 and

phase 7 of JJA BSISO1 for 1981–1998, 1999–2008, and 2009–2020, respectively (Fig. 12). By comparing with Fig. 2, the areas of negative SIC anomaly in Fig. 12b, c are like those in Fig. 2c. Especially from 2009 to 2020, there was a more significant negative correlation between the DJF SIC in the key region and the frequency of phase 3. During 1981–1998, the SIC-positive anomaly mainly was located at the junction of the mainland and the Arctic Ocean. For phase 7, the positive correlation between its frequency and DJF SIC was also more significant after 2009. Before 1998, no SIC anomaly related to phase 7 of BSISO1 was detected. These results inspired us to explore the potential mechanism of interdecadal changes.

Additionally, Lee et al. (2013) demonstrated in their study that there are two centres of variability for the ISO in the ASM region during summer: one in the South China Sea, the Philippine Sea and the other in the tropical Indian Ocean. However, the current study primarily focused on examining the impact of Arctic SIC on the BSISO and their associated physical processes over the western North Pacific. Incorporating this aspect into future research will enhance the theoretical understanding of how the Arctic influences the BSISO in the ASM region.

**Acknowledgements** This work is sponsored jointly by the National Key R&D Program of China (2022YFF0801702), the National Natural Science Foundation of China (41975090), the Natural Science Foundation of Hunan Province, China (2022JJ20043), the science and technology innovation Program of Hunan Province (2022RC1239), and the Jiangsu Collaborative Innovation Center for Climate Change in Nanjing University.

**Author contributions** All authors contributed to the study conception and design. Formal analysis and investigation were performed by Yao

Ha. Conceptualization was performed by Yimin Zhu. Methodology was performed by Yijia Hu. Supervision was performed by Zhong Zhong. The first draft of the manuscript was written by Zihuang Xie and all authors commented on previous versions of the manuscript. All authors read and approved the final manuscript.

**Funding** This work was supported by the National Key R&D Program of China (2022YFF0801702), the National Natural Science Foundation of China (41975090), the Natural Science Foundation of Hunan Province, China (2022JJ20043), the science and technology innovation Program of Hunan Province (2022RC1239).

**Data availability** The NCEP Reanalysis data are obtained from <https://psl.noaa.gov/data/gridded/data.ncep.reanalysis.html>. The HadISST data are obtained from <https://www.metoffice.gov.uk/hadobs/hadisst/>. The OLR data are obtained from <https://psl.noaa.gov/data/gridded/data.olrcdr.interp.html>. The BSISO indices are obtained from <https://apcc21.org/ser/moni.do?lang=en>. The Niño3.4 index is obtained from <https://psl.noaa.gov/data/correlation/nina34.anom.data>.

## Declarations

**Competing interests** The authors have no relevant financial or non-financial interests to disclose.

**Open Access** This article is licensed under a Creative Commons Attribution 4.0 International License, which permits use, sharing, adaptation, distribution and reproduction in any medium or format, as long as you give appropriate credit to the original author(s) and the source, provide a link to the Creative Commons licence, and indicate if changes were made. The images or other third party material in this article are included in the article's Creative Commons licence, unless indicated otherwise in a credit line to the material. If material is not included in the article's Creative Commons licence and your intended use is not permitted by statutory regulation or exceeds the permitted use, you will need to obtain permission directly from the copyright holder. To view a copy of this licence, visit <http://creativecommons.org/licenses/by/4.0/>.

## References

- Ajayamohan RS, Goswami BN (2007) Dependence of simulation of boreal summer tropical intraseasonal oscillations on the simulation of seasonal mean. *J Atmospheric Sci* 64:460–478. <https://doi.org/10.1175/JAS3844.1>
- Anderson JR, Rosen RD (1983) The latitude-height structure of 40–50 day variations in atmospheric angular momentum. *J Atmospheric Sci* 40:1584–1591. [https://doi.org/10.1175/1520-0469\(1983\)040:1584:CO;2](https://doi.org/10.1175/1520-0469(1983)040<1584:CO;2)
- Ashok K, Guan Z, Yamagata T (2003) A look at the relationship between the ENSO and the Indian Ocean Dipole. *J Meteorol Soc Jpn Ser II* 81(1):41–56. <https://doi.org/10.2151/jmsj.81.41>
- Barnes EA, Screen JA (2015) The impact of Arctic warming on the midlatitude jet-stream: can it? Has it? Will it? *WIREs Clim Change* 6:277–286. <https://doi.org/10.1002/wcc.337>
- Bellon G, Sobel AH (2008) Instability of the axisymmetric monsoon flow and intraseasonal oscillation. *J Geophys Res* 113:D07108. <https://doi.org/10.1029/2007JD009291>
- Bintanja R, Van Der Linden EC (2013) The changing seasonal climate in the Arctic. *Sci Rep* 3:1556. <https://doi.org/10.1038/srep01556>
- Boeke RC, Taylor PC (2018) Seasonal energy exchange in sea ice retreat regions contributes to differences in projected Arctic warming. *Nat Commun* 9:5017. <https://doi.org/10.1038/s41467-018-07061-9>
- Chen G, Wang B (2021) Diversity of the boreal summer intraseasonal oscillation. *J Geophys Res Atmospheres* 126:e2020JD034137. <https://doi.org/10.1029/2020JD034137>
- Chen S, Chen W, Wu R, Yu B, Graf H-F (2020) Potential impact of preceding aleutian low variation on El Niño-Southern oscillation during the following winter. *J Clim* 33:3061–3077. <https://doi.org/10.1175/JCLI-D-19-0717.1>
- Chen S, Chen W, Yu B, Wu L, Chen L, Li Z, Aru H, Huangfu J (2023a) Impact of the winter Arctic sea ice anomaly on the following summer tropical cyclone genesis frequency over the western North Pacific. *ClimDyn*. <https://doi.org/10.1007/s00382-023-06789-5>
- Chen S, Chen W, Yu B, Wu R (2023b) How well can current climate models simulate the connection of the early spring aleutian low to the following winter ENSO? *J Clim* 36:603–624. <https://doi.org/10.1175/JCLI-D-22-0323.1>
- Chen S, Chen W, Yu B, Wu R, Graf H-F, Chen L (2023c) Enhanced impact of the Aleutian Low on increasing the Central Pacific ENSO in recent decades. *NpjClim Atmos Sci* 6:1–13. <https://doi.org/10.1038/s41612-023-00350-1>
- Chripko S, Msadek R, Sanchez-Gomez E, Terray L, Bessières L, Moine M-P (2021) Impact of reduced Arctic sea ice on northern hemisphere climate and weather in autumn and winter. *J Clim* 1–61. <https://doi.org/10.1175/JCLI-D-20-0515.1>
- Cohen J et al (2014) Recent Arctic amplification and extreme mid-latitude weather. *Nat Geosci* 7:627–637. <https://doi.org/10.1038/ngeo2234>
- Cohen J et al (2020) Divergent consensus on Arctic amplification influence on midlatitude severe winter weather. *Nat Clim Change* 10:20–29. <https://doi.org/10.1038/s41558-019-0662-y>
- Comiso JC, Hall DK (2014) Climate trends in the Arctic as observed from space. *Wires Clim Change* 5:389–409. <https://doi.org/10.1002/wcc.277>
- Coumou D, Di Capua G, Vavrus S, Wang L, Wang S (2018) The influence of Arctic amplification on mid-latitude summer circulation. *Nat Commun* 9:2959. <https://doi.org/10.1038/s41467-018-05256-8>
- DeMott CA, Stan C, Randall DA (2013) Northward propagation mechanisms of the boreal summer intraseasonal oscillation in the ERA-Interim and SP-CCSM. *J Clim* 26:1973–1992. <https://doi.org/10.1175/JCLI-D-12-00191.1>
- Deng L, Li T (2016) Relative roles of background moisture and vertical shear in regulating interannual variability of boreal summer intraseasonal oscillations. *J Clim* 29:7009–7025. <https://doi.org/10.1175/JCLI-D-15-0498.1>
- Ding Q, Wang B (2005) Circumglobal teleconnection in the Northern Hemisphere summer. *J Clim* 18:3483–3505. <https://doi.org/10.1175/JCLI3473.1>
- Ding Q, Wang B (2009) Predicting extreme phases of the Indian Summer Monsoon. *J Clim* 22:346–363. <https://doi.org/10.1175/2008JCLI2449.1>
- Dixit V, Srinivasan J (2011) The role of vertical shear of the meridional winds in the northward propagation of ITCZ. *Geophys Res Lett* 38:L08812. <https://doi.org/10.1029/2010GL046601>
- Duan A et al (2022) Sea ice loss of the Barents-Kara Sea enhances the winter warming over the Tibetan Plateau. *Npj Clim Atmos Sci* 5:26. <https://doi.org/10.1038/s41612-022-00245-7>
- England MR, Polvani LM, Sun L, Deser C (2020) Tropical climate responses to projected Arctic and Antarctic sea-ice loss. *Nat Geosci* 13:275–281. <https://doi.org/10.1038/s41561-020-0546-9>
- Flatau M, Kim Y-J (2013) Interaction between the MJO and Polar Circulations. *J Clim* 26:3562–3574. <https://doi.org/10.1175/JCLI-D-11-00508.1>



- Francis JA, Vavrus SJ (2012) Evidence linking Arctic amplification to extreme weather in mid-latitudes. *Geophys Res Lett* 39:L06801. <https://doi.org/10.1029/2012GL051000>
- Fu H, Zhan R, Wu Z, Wang Y, Zhao J (2021) How does the Arctic sea ice affect the interannual variability of tropical cyclone activity over the Western North Pacific? *Front Earth Sci* 9:675150. <https://doi.org/10.3389/feart.2021.675150>
- Guan W, Hu H, Ren X, Yang X-Q (2019) Subseasonal zonal variability of the western Pacific subtropical high in summer: climate impacts and underlying mechanisms. *Clim Dyn* 53:3325–3344. <https://doi.org/10.1007/s00382-019-04705-4>
- He X, Zhang R, Ding S, Zuo Z (2021) Interdecadal linkage between the Winter Northern Hemisphere climate and Arctic sea ice of diverse location and seasonality. *Front Earth Sci* 9:758619. <https://doi.org/10.3389/feart.2021.758619>
- He W, Sun B, Ma J, Wang H (2022) Interdecadal variation in atmospheric water vapour content over East Asia during winter and the relationship with autumn Arctic sea ice. *Int J Climatol* 42:8868–8881. <https://doi.org/10.1002/joc.7779>
- Hersbach H et al (2020) The ERA5 global reanalysis. *Q J R Meteorol Soc* 146:1999–2049. <https://doi.org/10.1002/qj.3803>
- Holland MM, Bitz CM (2003) Polar amplification of climate change in coupled models. *Clim Dyn* 21:221–232. <https://doi.org/10.1007/s00382-003-0332-6>
- Holland MM, Bitz CM, Tremblay B (2006) Future abrupt reductions in the summer Arctic sea ice. *Geophys Res Lett* 33:L23503. <https://doi.org/10.1029/2006GL028024>
- Honda M, Inoue J, Yamane S (2009) Influence of low Arctic sea-ice minima on anomalously cold Eurasian winters. *Geophys Res Lett* 36:L08707. <https://doi.org/10.1029/2008GL037079>
- Hu H, Wang R, Liu F, Perrie W, Fang J, Bai H (2022) Cumulative positive contributions of propagating ISO to the quick low-level atmospheric response during El Niño developing years. *Clim Dyn* 58:569–590. <https://doi.org/10.1007/s00382-021-05924-4>
- Hu H, Li Y, Yang X, Wang R, Mao K, Yu P (2023) Influences of oceanic processes between the Indian and Pacific Basins on the Eastward propagation of MJO events crossing the maritime continent. *J Geophys Res Atmos* 128:e2022JD038239. <https://doi.org/10.1029/2022JD038239>
- Huang KM, Coauthors (2015) Observational evidence of quasi-27-day oscillation propagating from the lower atmosphere to the mesosphere over 20° N. *Ann Geophys* 33:1321–1330. <https://doi.org/10.5194/angeo-33-1321-2015>
- Jiang X, Li T, Wang B (2004) Structures and mechanisms of the northward propagating boreal summer intraseasonal oscillation\*. *J Clim* 17:1022–1039. [https://doi.org/10.1175/1520-0442\(2004\)017%3c1022:SAMOTN%3e2.0.CO;2](https://doi.org/10.1175/1520-0442(2004)017%3c1022:SAMOTN%3e2.0.CO;2)
- Kajikawa Y, Yasunari T, Wang B (2009) Decadal change in intraseasonal variability over the South China Sea. *Geophys Res Lett* 36:L06810. <https://doi.org/10.1029/2009GL037174>
- Kang I-S, Ho C-H, Lim Y-K, Lau K-M (1999) Principal modes of climatological seasonal and intraseasonal variations of the Asian Summer Monsoon. *Mon Weather Rev* 127:322–340. [https://doi.org/10.1175/1520-0493\(1999\)127%3c0322:PMOCSA%3e2.0.CO;2](https://doi.org/10.1175/1520-0493(1999)127%3c0322:PMOCSA%3e2.0.CO;2)
- Kikuchi K (2021) The Boreal Summer Intraseasonal Oscillation (BSISO): a review. *J Meteorol Soc Jpn Ser II* 99:933–972. <https://doi.org/10.2151/jmsj.2021-045>
- Kikuchi K, Wang B (2010) Formation of tropical cyclones in the northern Indian Ocean associated with two types of tropical intraseasonal oscillation modes. *J Meteorol Soc Jpn Ser II* 88:475–496. <https://doi.org/10.2151/jmsj.2010-313>
- Kim H, Yeh S, An S, Park J, Kim B, Baek E (2020) Arctic sea ice loss as a potential trigger for Central Pacific El Niño events. *Geophys Res Lett* 47:e2020GL087028. <https://doi.org/10.1029/2020GL087028>
- Krishnamurthy V, Shukla J (2008) Seasonal persistence and propagation of intraseasonal patterns over the Indian monsoon region. *Clim Dyn* 30:353–369. <https://doi.org/10.1007/s00382-007-0300-7>
- Lee J-Y et al (2010) How are seasonal prediction skills related to models' performance on mean state and annual cycle? *Clim Dyn* 35:267–283. <https://doi.org/10.1007/s00382-010-0857-4>
- Lee J-Y, Wang B, Wheeler MC, Fu X, Waliser DE, Kang I-S (2013) Real-time multivariate indices for the boreal summer intraseasonal oscillation over the Asian summer monsoon region. *Clim Dyn* 40:493–509. <https://doi.org/10.1007/s00382-012-1544-4>
- Li Y, Leung LR (2013) Potential impacts of the Arctic on interannual and interdecadal summer precipitation over China. *J Clim* 26:899–917. <https://doi.org/10.1175/JCLI-D-12-00075.1>
- Li K, Yu W, Li T, Murty VSN, Khokiattiwong S, Adi TR, Budi S (2013) Structures and mechanisms of the first-branch northward-propagating intraseasonal oscillation over the tropical Indian Ocean. *Clim Dyn* 40:1707–1720. <https://doi.org/10.1007/s00382-012-1492-z>
- Li M, Luo D, Simmonds I, Dai A, Zhong L, Yao Y (2021) Anchoring of atmospheric teleconnection patterns by Arctic Sea ice loss and its link to winter cold anomalies in East Asia. *Int J Climatol* 41:547–558. <https://doi.org/10.1002/joc.6637>
- Li Y, Zhang L, Gan B, Wang H, Li X, Wu L (2023) Observed contribution of Barents-Kara sea ice loss to warm Arctic-cold Eurasia anomalies by submonthly processes in winter. *Environ Res Lett* 18:034019. <https://doi.org/10.1088/1748-9326/acbb92>
- Liu F, Wang B (2016) Role of horizontal advection of seasonal-mean moisture in the Madden-Julian oscillation: a theoretical model analysis. *J Clim* 29:6277–6293. <https://doi.org/10.1175/JCLI-D-16-0078.1>
- Liu J, Curry JA, Wang H, Song M, Horton RM (2012) Impact of declining Arctic sea ice on winter snowfall. *Proc Natl Acad Sci* 109:4074–4079. <https://doi.org/10.1073/pnas.1114910109>
- Liu J, Song M, Horton RM, Hu Y (2013) Reducing spread in climate model projections of a September ice-free Arctic. *Proc Natl Acad Sci* 110:12571–12576. <https://doi.org/10.1073/pnas.1219716110>
- Liu J, Song M, Zhu Z, Horton RM, Hu Y, Xie S-P (2022) Arctic sea-ice loss is projected to lead to more frequent strong El Niño events. *Nat Commun* 13:4952. <https://doi.org/10.1038/s41467-022-32705-2>
- Ma J, Wang H, Zhang Y (2014) Will typhoon over the western North Pacific be more frequent in the Blue Arctic conditions? *Sci. China Earth Sci* 57:1494–1500. <https://doi.org/10.1007/s11430-013-4747-6>
- Madden RA, Julian PR (1994) Observations of the 40–50-day tropical oscillation—a review. *Mon Weather Rev* 122:814–837. [https://doi.org/10.1175/1520-0493\(1994\)122<0814:OOTDTP>2.0.CO;2](https://doi.org/10.1175/1520-0493(1994)122<0814:OOTDTP>2.0.CO;2)
- Mori M, Watanabe M, Shioyama H, Inoue J, Kimoto M (2014) Robust Arctic sea-ice influence on the frequent Eurasian cold winters in past decades. *Nat Geosci* 7:869–873. <https://doi.org/10.1038/ngeo2277>
- Nakano M, Vitart F, Kikuchi K (2021) Impact of the Boreal summer intraseasonal oscillation on typhoon tracks in the western North Pacific and the prediction skill of the ECMWF Model. *Geophys Res Lett* 48:L091505. <https://doi.org/10.1029/2020GL091505>
- Pancheva D (2003) Intra-seasonal oscillations observed in the MLT region above UK (52°N, 2°W) and ESRANGE (68°N, 21°E). *Geophys Res Lett* 30:2084. <https://doi.org/10.1029/2003GL017809>
- Perovich DK, Richter-Menge JA, Jones KF, Light B (2008) Sunlight, water, and ice: extreme Arctic sea ice melt during the summer of 2007. *Geophys Res Lett* 35:2008GL034007. <https://doi.org/10.1029/2008GL034007>

- Pithan F, Mauritsen T (2014) Arctic amplification dominated by temperature feedbacks in contemporary climate models. *Nat Geosci* 7. <https://doi.org/10.1038/NNGEO2071>
- Plumb RA (1985) On the three-dimensional propagation of stationary waves. *J Atmos Sci* 42:217–229. [https://doi.org/10.1175/1520-0469\(1985\)042%3c0217:OTTDPO%3e2.0.CO;2](https://doi.org/10.1175/1520-0469(1985)042%3c0217:OTTDPO%3e2.0.CO;2)
- Qian S, Hu H, Ren X, Yang X-Q, Yu P, Mao K (2023) Synergistic effects of upstream disturbances and oceanic fronts on the sub-seasonal evolution of Western Pacific Jet Stream in winter. *J Geophys Res Atmos* 128:e2022JD038331. <https://doi.org/10.1029/2022JD038331>
- Rampal P, Weiss J, Dubois C, Campin J-M (2011) IPCC climate models do not capture Arctic sea ice drift acceleration: Consequences in terms of projected sea ice thinning and decline. *J Geophys Res* 116:C00D07. <https://doi.org/10.1029/2011JC007110>
- Rantanen M, Karpechko AY, Lipponen A, Nordling K, Hyvärinen O, Ruosteenoja K, Vihma T, Laaksonen A (2022) The Arctic has warmed nearly four times faster than the globe since 1979. *Commun Earth Environ* 3:168. <https://doi.org/10.1038/s43247-022-00498-3>
- Rosenblum E, Eisenman I (2017) Sea ice trends in climate models only accurate in runs with biased global warming. *J Clim* 30:6265–6278. <https://doi.org/10.1175/JCLI-D-16-0455.1>
- Sang X, Yang X-Q, Tao L, Fang J, Sun X (2022) Decadal changes of wintertime poleward heat and moisture transport associated with the amplified Arctic warming. *Clim Dyn* 58:137–159. <https://doi.org/10.1007/s00382-021-05894-7>
- Serra YL, Jiang X, Tian B, Amador-Astua J, Maloney ED, Kiladis GN (2014) Tropical intraseasonal modes of the atmosphere. *Annu Rev Environ Resour* 39:189–215. <https://doi.org/10.1146/annurev-environ-020413-134219>
- Screen JA (2017) Far-flung effects of Arctic warming. *Nat Geosci* 10:253–254. <https://doi.org/10.1038/ngeo2924>
- Screen JA, Simmonds I (2013) Exploring links between Arctic amplification and mid-latitude weather. *Geophys Res Lett* 40:959–964. <https://doi.org/10.1002/grl.50174>
- Screen JA, Deser C, Simmonds I, Tomas R (2014) Atmospheric impacts of Arctic sea-ice loss, 1979–2009: separating forced change from atmospheric internal variability. *Clim Dyn* 43:333–344. <https://doi.org/10.1007/s00382-013-1830-9>
- Sigmond M, Fyfe JC, Swart NC (2018) Ice-free Arctic projections under the Paris Agreement. *Nat Clim Change* 8:404–408. <https://doi.org/10.1038/s41558-018-0124-y>
- Stroeve J, Holland MM, Meier W, Scambos T, Serreze M (2007) Arctic sea ice decline: Faster than forecast. *Geophys Res Lett* 34. <https://doi.org/10.1029/2007GL029703>
- Sun C, Liu Y, Zhang J (2020) Roles of sea surface temperature warming and loss of Arctic Sea ice in the enhanced summer wetting trend over Northeastern Siberia during recent decades. *J Geophys Res Atmospheres* 125. <https://doi.org/10.1029/2020JD032557>
- Takaya K, Nakamura H (2001) A formulation of a phase-independent wave-activity flux for stationary and migratory quasigeostrophic eddies on a zonally varying basic flow. *J Atmos Sci* 58:608–627. [https://doi.org/10.1175/1520-0469\(2001\)058%3c0608:AFOAPI%3e2.0.CO;2](https://doi.org/10.1175/1520-0469(2001)058%3c0608:AFOAPI%3e2.0.CO;2)
- Vihma T (2014) Effects of Arctic sea ice decline on weather and climate: a review. *Surv Geophys* 35. <https://doi.org/10.1007/s10712-014-9284-0>
- Walsh JE (1980) Empirical orthogonal function and the statistical predictability of sea ice. University of Washington Press
- Wang B, Ding Q (2008) Global monsoon: dominant mode of annual variation in the tropics. *Dyn Atmos Oceans* 44:165–183. <https://doi.org/10.1016/j.dynatmoce.2007.05.002>
- Wang B, Xie X (1996) Low-frequency equatorial waves in vertically sheared zonal flow. Part I: stable waves. *J Atmos Sci* 53:449–467. [https://doi.org/10.1175/1520-0469\(1996\)053%3c0449:LFE-WIV%3e2.0.CO;2](https://doi.org/10.1175/1520-0469(1996)053%3c0449:LFE-WIV%3e2.0.CO;2)
- Wang B, Webster PJ, Teng H (2005) Antecedents and self-induction of active-break south Asian monsoon unraveled by satellites. *Geophys Res Lett* 32:L04704. <https://doi.org/10.1029/2004GL020996>
- Wang B, Webster P, Kikuchi K, Yasunari T, Qi Y (2006) Boreal summer quasi-monthly oscillation in the global tropics. *Clim Dyn* 27:661–675. <https://doi.org/10.1007/s00382-006-0163-3>
- Wang B et al (2009) Advance and prospectus of seasonal prediction: assessment of the APCC/ClipAS 14-model ensemble retrospective seasonal prediction (1980–2004). *Clim Dyn* 33:93–117. <https://doi.org/10.1007/s00382-008-0460-0>
- Wang H, Wang B, Huang F, Ding Q, Lee J-Y (2012) Interdecadal change of the boreal summer circumglobal teleconnection (1958–2010). *Geophys Res Lett* 39:L12704. <https://doi.org/10.1029/2012GL052371>
- Wang F, Han Y, Zhang S, Zhang R (2020) Influence of stratospheric sudden warming on the tropical intraseasonal convection. *Environ Res Lett* 15:084027. <https://doi.org/10.1088/1748-9326/ab98b5>
- Wang F, Huang R, Wang L (2022) Response of tropical convection over the western Pacific to stratospheric polar vortex during boreal winter. *Int J Climatol* 42:9886–9896. <https://doi.org/10.1002/joc.7869>
- Wang Y, Hu H, Ren X, Yang X-Q, Mao K (2023) Significant northward jump of the western Pacific subtropical high: the interannual variability and mechanisms. *J Geophys Res Atmos* 128:e2022JD037742. <https://doi.org/10.1029/2022JD037742>
- Webster PJ, Magaña VO, Palmer TN, Shukla J, Tomas RA, Yanai M, Yasunari T (1998) Monsoons: processes, predictability, and the prospects for prediction. *J Geophys Res Oceans* 103:14451–14510. <https://doi.org/10.1029/97JC02719>
- Wei K, Liu J, Bao Q, He B, Ma J, Li M, Song M, Zhu Z (2021) Sub-seasonal to seasonal Arctic sea-ice prediction: a grand challenge of climate science. *Atmos Ocean Sci Lett* 14:21–23. <https://doi.org/10.1016/j.aosl.2021.100052>
- Wei X, Chen L, Chen M, Lei Y (2022) Modulation of boreal summer intraseasonal oscillation on tropical cyclone genesis over the South China Sea. *Meteorol Atmos Phys* 134:62. <https://doi.org/10.1007/s00703-022-00901-w>
- Wheeler MC, Hendon HH (2004) An all-season real-time Multivariate MJO Index: development of an index for monitoring and prediction. *Mon Weather Rev* 132:1917–1932. [https://doi.org/10.1175/1520-0493\(2004\)132%3c1917:AARMMI%3e2.0.CO;2](https://doi.org/10.1175/1520-0493(2004)132%3c1917:AARMMI%3e2.0.CO;2)
- Wu R, Cao X (2017) Relationship of boreal summer 10–20-day and 30–60-day intraseasonal oscillation intensity over the tropical western North Pacific to tropical Indo-Pacific SST. *Clim Dyn* 48:3529–3546. <https://doi.org/10.1007/s00382-016-3282-5>
- Wu B, Zhang R, Wang B (2009a) On the association between spring Arctic sea ice concentration and Chinese summer rainfall: a further study. *Adv Atmos Sci* 26:666–678. <https://doi.org/10.1007/s00376-009-9009-3>
- Wu B, Zhang R, Wang B, D'Arrigo R (2009b) On the association between spring Arctic sea ice concentration and Chinese summer rainfall. *Geophys Res Lett* 36:L09501. <https://doi.org/10.1029/2009GL037299>
- Wu B, Zhang R, D'Arrigo R, Su J (2013) On the relationship between winter sea ice and summer atmospheric circulation over Eurasia. *J Clim* 26:5523–5536. <https://doi.org/10.1175/JCLI-D-12-00524.1>

- Xie X, Wang B (1996) Low-frequency equatorial waves in vertically sheared zonal flow. Part II: unstable waves. *J Atmos Sci* 53:3589–3605. [https://doi.org/10.1175/1520-0469\(1996\)053%3c3589:LFEWIV%3e2.0.CO;2](https://doi.org/10.1175/1520-0469(1996)053%3c3589:LFEWIV%3e2.0.CO;2)
- Yamaura T, Kajikawa Y (2017) Decadal change in the boreal summer intraseasonal oscillation. *Clim Dyn* 48:3003–3014. <https://doi.org/10.1007/s00382-016-3247-8>
- Yang S, Li T (2016) Intraseasonal variability of air temperature over the mid-high latitude Eurasia in boreal winter. *Clim Dyn* 47:2155–2175. <https://doi.org/10.1007/s00382-015-2956-8>
- Yang X, Zeng G, Zhang G, Li Z (2020) Interdecadal variation of winter cold surge path in east Asia and its relationship with Arctic sea ice. *J Clim* 33:4907–4925. <https://doi.org/10.1175/JCLI-D-19-0751.1>
- Yao Y, Coauthors (2023) Extreme cold events in North America and Eurasia in November–December 2022: a potential vorticity gradient perspective. *Adv Atmospheric Sci* 40:953–962. <https://doi.org/10.1007/s00376-023-2384-3>
- Yuan X, Kaplan MR, Cane MA (2018) The Interconnected global climate system—a review of tropical-polar teleconnections. *J Clim* 31:5765–5792. <https://doi.org/10.1175/JCLI-D-16-0637.1>
- Zhang C (2005) Madden-Julian oscillation. *Rev Geophys* 43:RG2003. <https://doi.org/10.1029/2004RG000158>
- Zhang C (2013) Madden–Julian oscillation: bridging weather and climate. *Bull Am Meteorol Soc* 94:1849–1870. <https://doi.org/10.1175/BAMS-D-12-00026.1>
- Zhou B, Qian J, Hu Y, Li H, Han T, Sun B (2023) Interdecadal change in the linkage of early summer sea ice in the Barents Sea to the variability of West China Autumn Rain. *Atmos Res* 287:106717. <https://doi.org/10.1016/j.atmosres.2023.106717>

**Publisher's Note** Springer Nature remains neutral with regard to jurisdictional claims in published maps and institutional affiliations.